KERNFORSCHUNGSZENTRUM

KARLSRUHE

November 1976   KFK 2366

Evaporation Studies of Liquid Oxide Fuel at Very High Temperatures Using Laser Beam Heating

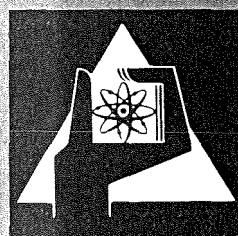M. Bober, W. Breitung, H. U. Karow, K. Schretzmann

KERNFORSCHUNGSZENTRUM KARLSRUHE

KFK 2366

Institut für Neutronenphysik und Reaktortechnik
Projekt Schneller Brüter

Evaporation Studies of Liquid Oxide Fuel at Very High Tempera-
tures Using Laser Beam Heating

M.Bober, W.Breitung, H.U.Karow, K.Schretzmann

Abstract

Safety analysis of fast reactors requires knowledge of the evaporation behavior and the total vapor pressure of oxide fuel materials in the temperature region from 3000 K upwards. Therefore, evaporation experiments with oxide fuel are carried out based on laser beam heating of the fuel specimen surface. Rectangular laser pulses of 1 to 10 msec pulse length are used, cut out from the continuous beam of a high-power CO_2 laser. The measuring quantities are the recoil momentum of the target, the evaporation area, the evaporation time and the mass and momentum of the supersonic vapor jet expanding into vacuum, and the thermal radiation density of the evaporating surface. From the mechanical measuring quantities we derive the vapor pressure of the target material and, in a first approach, also the evaporation temperature by applying a gas dynamic evaluation model. In a second approach, after having measured the spectral emissivity of liquid UO_2 at 633 nm by use of a He-Ne laser, we determine the evaporation temperature at the liquid surface also from its thermal radiation. For the determination of the vapor pressure from the measured quantities a gas dynamic evaluation model has been developed. An application limit of the measuring technique is given by onset of plasma interaction of the vapor plume with the incident laser beam at temperatures above 4500 K. Movement of liquid material in the laser crater caused by the reactor pressure of the vapor jet does not disturb the vapor pressure measurements.

The dynamic vapor pressure measurements on liquid oxide fuels with laser heating techniques imply strong alternations in the composition of the incongruently evaporating fuel surface, since, during open evaporation, the depletion in the preferentially evaporating components cannot be restored by diffusion from the bulk material. After a short transient evaporation period stationary surface-evaporation is reached with a surface composition which differs greatly

from the given fuel composition and depends on the actual evaporation temperature. When this stationary forced-congruent evaporation mode is reached, the gross vapor composition is well-defined and is identical to the bulk composition of the fuel but is quite different from the actual surface composition. In consequence, the total vapor pressure developing in open surface-evaporation of a liquid oxide fuel can substantially deviate from its thermodynamic equation-of-state, in the case of $(U_{0.80}Pu_{0.20})$ mixed oxide by a factor of 2 to 7 depending on the O/M-ratio. The required equation-of-state of liquid mixed oxide, however, can be deduced in a further step from the vapor pressure curve measured in open evaporation by thermodynamic calculations.

Experimental values for the saturated vapor pressure of UO_2 are presented, determined from three series of laser evaporation measurements obtained at temperatures around 3500 K, 3950 K, and 4200 K. The average vapor pressures found are .6 bar, 3 bar, and 7 bar, respectively. Laser vapor pressure measurements performed by other authors and theoretical extrapolations of the UO_2 vapor pressure curve known from literature show fairly good agreement within their confidence interval with the vapor pressure measurements reported here.

Verdampfungsuntersuchungen an flüssigem Oxidbrennstoff mittels
Laserheizung bei sehr hohen Temperaturen.

Kurzfassung

Für die Sicherheitsanalyse schneller Reaktoren werden ver-
läßliche Aussagen und Daten zum Verdampfungsverhalten und
zum Dampfdruck von Oxidbrennstoff bei Temperaturen oberhalb
3000 K benötigt. Deshalb werden Laserverdampfungsexperimente
mit Oxidbrennstoff durchgeführt, bei denen die Brennstoff-
oberfläche mit einem fokussierten Laserstrahl lokal aufge-
heizt wird. Hierfür werden Laserpulse von 1 bis 10 ms Puls-
länge verwendet, die mit dem kontinuierlichen Strahl eines
Hochleistungs-CO_2-Lasers erzeugt werden. Die Meßgrößen sind:
Rückstoßimpuls des Targets, Verdampfungsfläche, Verdampfungs-
zeit, Masse und Vorwärtsimpuls des ins Vakuum expandierenden
Überschall-Dampfstrahls, und die thermische Strahlungsdichte
der verdampfenden Oberfläche. Aus den mechanischen Meßgrößen
wird der Dampfdruck des untersuchten Materials ermittelt, und
in einer ersten Auswertung mit Hilfe eines gasdynamischen
Modells auch die Verdampfungstemperatur. Nach Messung des
spektralen Emissionsvermögens des flüssigen Brennstoffs bei
der Wellenlänge des He-Ne-Lasers (633 nm) wird in einer
zweiten Auswertung die Temperatur an der verdampfenden Brenn-
stoffoberfläche zusätzlich aus deren thermischer Strahlungs-
dichte ermittelt. Die Bestimmung des Dampfdrucks erfolgt mit
einem gasdynamischen Auswertemodell. Eine Anwendungsgrenze
des Meßverfahrens ist dadurch gegeben, daß bei Temperaturen
über 45oo K mit einer starken Plasmawechselwirkung des
einfallenden Laserstrahls mit der erzeugten Dampfwolke zu
rechnen ist. Hingegen stört die vom Rückstoßdruck des Dampf-
strahls hervorgerufene Flüssigkeitsbewegung im Brennfleck
die Dampfdruckmessung nicht.

Eine dynamische Dampfdruckmessung, bei der wie im vorliegen-
den Fall flüssiger Oxidbrennstoff offen verdampft wird,
impliziert starke Veränderungen in der Zusammensetzung der
jeweils inkongruent verdampfenden Brenstoffoberfläche. Die

mit der intensiven Verdampfung verbundene Verarmung in der
Oberfläche an den überproportional verdampfenden Komponenten
kann durch Nachdiffusion aus der kondensierten Phase nicht
ausgeglichen werden. Nach einer kurzen transienten Verdampfungs-
periode stellt sich mit der stationären Oberflächenverdampfung
eine Oberflächenzusammensetzung ein, die von der vorgegebenen
Brennstoffzusammensetzung stark abweicht und von der jeweiligen
Verdampfungstemperatur abhängt. Mit Erreichen dieses stationären,
aus Massenbilanzgründen erzwungen-kongruenten Verdampfungszu-
standes ist die Bruttozusammensetzung im Dampf genau gleich
der vorgegebenen Zusammensetzung des Brennstoffs, jedoch stark
verschieden von der jeweiligen Zusammensetzung der verdampfen-
den Oberfläche. Wegen dieser Entmischungsvorgänge in der
kondensierten Phase kann der Totaldampfdruck eines flüssigen
Oxidbrennstoffs bei offener Verdampfung wesentlich von seiner
thermodynamischen Zustandsgleichung abweichen, z.B. bei
$(U_{0.80}Pu_{0.20})$-Mischoxid um einen Faktor 2 bis 7, je nach
vorgegebenem O/M-Verhältnis. Die gesuchte Zustandsgleichung
des flüssigen Mischoxids kann jedoch in einem weiteren Schritt
mittels thermodynamischer Rechnungen aus der bei offener Ver-
dampfung gemessenen Dampfdruckkurve abgeleitet werden.

Experimentell ermittelte Dampfdruckdaten für UO_2, die in
drei Meßreihen aus Laserverdampfungsexperimenten bei Tempera-
turen um 3500 K, 3950 K und 4200 K gewonnen wurden, sind
angegeben. Die bei diesen Temperaturen gefundenen Dampfdrucke
betragen gemittelt 0,6 bar, 3 bar und 7 bar. Laserdampfdruck-
messungen anderer Autoren und die aus der Literatur bekannten
Extrapolationen der UO_2-Dampfdruckkurve stimmen innerhalb der
anzunehmenden Fehlerbreiten ziemlich gut mit den vorliegenden
Dampfdruckmessungen überein.

I. Introduction

Since some time there has been an increasing interest in vapor
pressure data of oxide fuel materials at very high temperatures.
This has been caused by the requirements of fast reactor safety
analysis. Complete analysis of hypothetical core disruptive
accidents requires knowledge of the equations of state of the
fuel at temperatures up to 5000 K or higher.

As shown in Fig.1, in the temperature range below the melting
point the vapor pressure over UO_2 has been the subject of
numerous investigations [1-9]. The methods used have been
Knudsen effusion, Langmuir free evaporation and the trans-
piration technique. A recently made theoretical extrapola-
tion [10] with new thermodynamic data [11] based on the law
of mass action is represented by the dashed line.

Until now there had been a lack of experimental investiga-
tions into the liquid region except for one experiment in-
volving temperatures up to 3400 K [9]. Above these tempera-
tures conventional measurements fail because no suitable
containment materials are available. Only non-static sur-
face-evaporation techniques can be applied, for example, by
local heating of the specimen surface with a pulsed laser
beam. Therefore, efforts have been made to determine the
vapor pressure of liquid oxide fuel from laser evaporation
experiments [12-14]. Such experiments are going on at our
Institute in the Karlsruhe Nuclear Research Center and also
at the European Institute for Transuranium Elements where
similar experiments with different measuring and evaluation
techniques are carried out by Ohse et al. [15-17].

These experiments are associated with several new problems.

Contrary to the isothermal measuring techniques, laser sur-
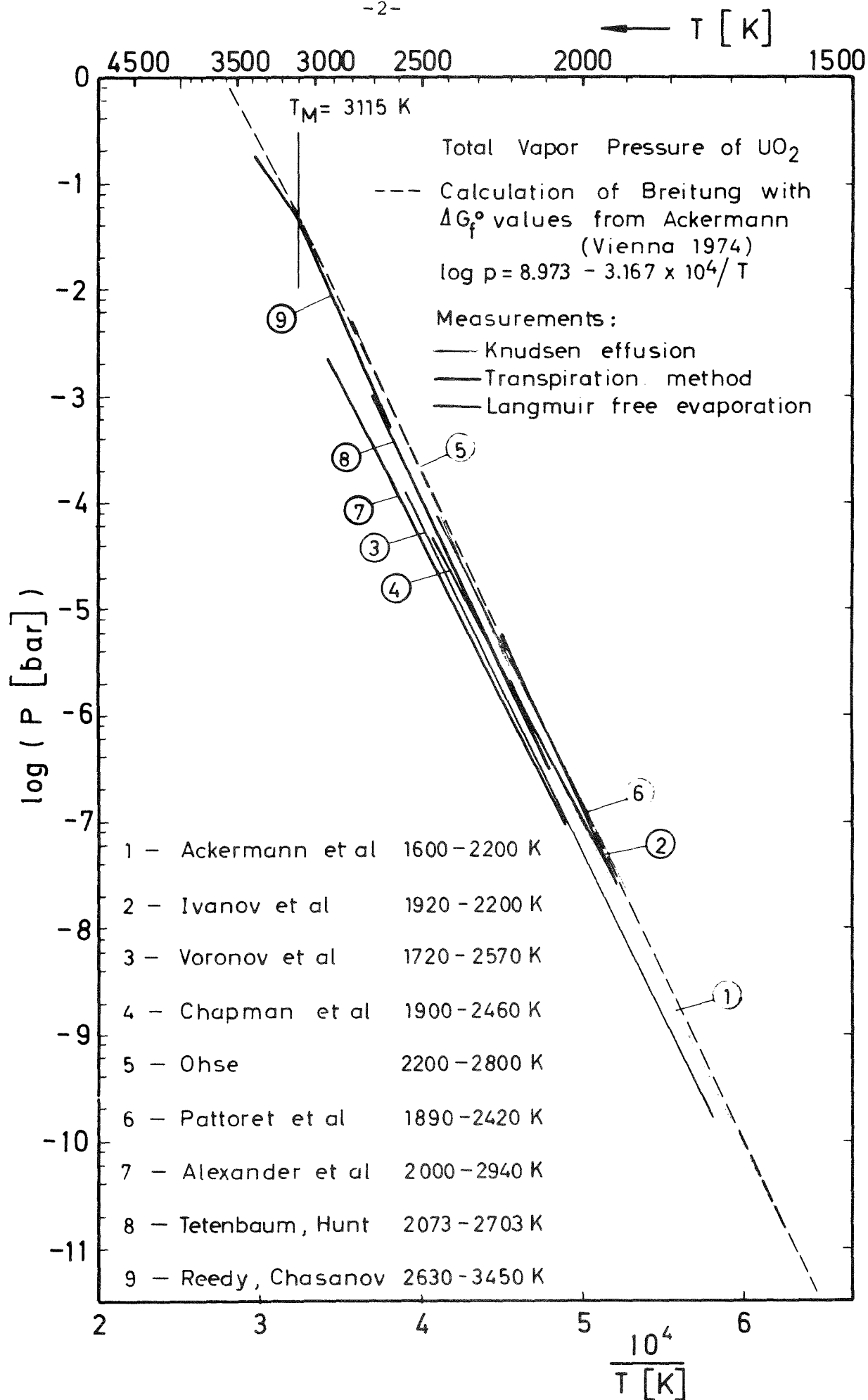face heating is characterized by high temperature gradients

Zum Druck eingereicht am

Fig. 1 Total vapor pressure of UO_2 below the melting point

within the surface layer of the specimen. These gradients
arise from the fact that the laser power is absorbed in a
thin layer below the target surface, which results in a dis-
tributed internal heat source, and the front surface is
intensively cooled by vaporization, which balances the ab-
sorbed laser power in steady state. Between temperatures of
4000 and 5000 K, e.g., evaporation of UO_2 implies a tempera-
ture gradient immediately below the evaporating surface going
from 100 K/μm to 1000 K/μm.

The laser generated vapor cloud near the target surface is
so dense that its state involves a gas dynamic vapor flow
off. Molecules leaving the surface have initially a Max-
wellian velocity distribution. During expansion of the vapor
into vacuum this distribution gradually changes with in-
creasing distance from the surface as the internal energy is
converted into forward motion. The gas molecules accelerate
to the local velocity of sound, and finally to supersonic
velocities [12].

The vapor jet, which flows off from the surface in the
form of a gasdynamic expansion, exerts a reaction pressure
on the evaporation surface which causes molten material to
move outward along the surface of the laser-produced crater.
This liquid displacement under certain conditions can cause
trouble in vapor pressure evaluation [18]. Furthermore, as in
all open evaporation experiments the insufficient knowledge
of the vaporization coefficient makes uncertain the determina-
tion of the saturated vapor pressure.

Another point is that in open evaporation òf liquid oxide
fuel the composition of the evaporating surface changes.
Incongruent evaporation leads to a strong depletion in the
preferentially evaporating components, which cannot be
restored by diffusion in the condensed phase during laser
impact. The actual vapor pressure over the surface can there-
fore depart appreciably from the equilibrium vapor pressure
of the given bulk material [19-22].

The principal restraint on these laser evaporation experiments is that laser heating itself should not disturb the measurements by strong interaction of the incident laser beam and the vapor jet. This determines an upper temperature limit of the experiments [12-14].

When dynamic measuring techniques based on laser pulse heating are applied, the total vapor pressure required has to be evaluated either from the surface evaporation rate of the specimen or from the reaction pressure exerted on the specimen by the vapor jet. The reaction pressure can be determined integrally e.g., by a simple ballistic pendulum device [12]. The evaporation rate results either from the mass loss of the specimen or from the laser produced crater depth. The mass loss can be determined by weighing, as we proceed in this way in our measurements [12], and the evaporation crater depth can be obtained by microscope inspection of the crater [15].

The determination of crater depth offers the advantage of a spatial resolution of the evaporation rate with respect to the power profile of the incident laser beam. But it is very sensitive to the liquid layer movement because the true evaporation effect on crater depth lies inthe µm-range. Therefore, this method is restricted to short laser pulses in the µs-range in order to avoid as far as possible liquid displacement.

The determination of reaction pressure and mass loss rate are practically not affected by liquid movement [18]. This allows to determine the vapor pressure from evaporation experiments using relatively long laser pulses.

An experimental difficulty lies in determination of the evaporation temperature. Unfortunately, there is no method known of measuring the temperature during the laser pulse, which can be used without reservations.

One possibility is to calculate the evaporation temperature
from the heat balance of the absorbed laser energy and the
heat removed by evaporation. This method assumes prior know-
ledge of the absorption coefficient of the laser light as
well as of the enthalpy and latent heat of vaporization of
the liquid. In addition, heat conduction and convectional
heat removal by liquid movement must be considered. A simp-
lified illustration of the heat balance is shown by Eq.(1).
It relates the absorbed laser power density P_{abs} to the molar
heat of evaporation H_v and the enthalpy content $\Delta H(T)$ of
the liquid.

$$(1) \qquad P_{abs} = \frac{\rho}{M} \left[v_{evap} \cdot H_v + (v_{evap} + v_{recession}) \cdot \Delta H(T_{evap}) \right]$$

ρ and M are the density and molecular weight, respectively,
of the evaporating material, v_{evap} is the evaporation velo-
city and $v_{recession}$ the velocity of the surface recession due
to liquid displacement.

Another way is to get information on the evaporation tempera-
ture from the final velocity of the vapor flow after its
gas dynamic expansion. This velocity is related to the actual
number of degrees of freedom taking part in the relaxation
into kinetic flow energy, which must be known sufficiently
well. It is an advantage that the temperature information
gained from the vapor jet in this way originates exactly
from the evaporating surface.

Spectroscopic methods can serve to determine the temperature
of the hot vapor plume, which however is not necessarily
identical with the temperature of the evaporating surface
because of the temperature decrease during adiabatic ex-
pansion of the vapor.

A practicable way of temperature measurement is by direct optical pyrometry. However, the problem must be solved of the unknown spectral emission coefficient. Besides, it is clear that the thermal radiation entering the pyrometer does not only originate from the evaporating surface but comes from a surface layer of a certain thickness. This means that the steep temperature gradient existing below the evaporating surface contributes to the thermal radiation of the liqued surface and thus complicates evaluation of the surface temperature. At extreme temperatures pyrometric temperature measurement becomes unreliable when in the ionized vapor plume the absorption of thermal radiation begins to become appreciable.

We turn now to the laser evaporation experiments with liquid UO_2 and discuss them in more detail.

Laser energy coupling to UO_2 has been proved to be very effective. It allows surface evaporation with beam intensities in the low power regime between some 10^4 and 10^6 W/cm^2. The application of longer laser pulses of such moderate power densities has some advantages. During laser heating true surface evaporation of the molten material takes place. Surface depletion effects and vapor flow conditions become stationary. Besides, it reduces the requirements to the laser systems.

The selected measuring method is based on the determination of the reaction pressure and the mass loss rate of the target specimen using a microbalance and a ballistic pendulum technique. Applying relatively low power densities and long evaporation periods up to the ms range this method allows to extend the measurements down to temperatures of about 3500 K, i.e. below the boiling point of UO_2 where the results are directly adjoining that from conventional measurements.

II. Experiments

We use a mechanically switched CO_2 laser beam to heat the specimen surface. The measured quantities are the recoil momentum of the target, the evaporation area, the evaporation time and the mass and momentum of the vapor jet expanding into a vacuum, and the thermal radiation of the evaporating surface. From the mechanical measuring quantities we determine the vapor pressure of the target material and, in a first approach, also the evaporation temperature by applying a gas dynamic evaluation model. In a second approach, after having measured the spectral emissivity of liquid UO_2 at 633 nm by use of a He-Ne-laser, we determine the evaporation temperature at the liquid surface also from its thermal radiation at 633 nm by use of a fast pyrometer.

The measuring principle is shown in Fig.2. The CO_2 laser emits a continuous beam in the transverse Gaussian mode at a wavelength of 10.6 μm. Its power output is very stable and adjustable up to 400 W. An electromagnetic chopper-shutter system cuts out from the continuous laser beam a 1 to 10 ms long pulse of exactly constant power. This well-defined rectangular laser pulse ensures defined and reproducible target heating. The target specimen is suspended as a ballistic pendulum from the pan of a microbalance in a vacuum chamber.

The laser beam is directed into the vacuum chamber by a mirror system and focused on the specimen surface by a ZnSe objective lens. By a special rotating wobble mirror the laser focus, during the pulse, can be uniformly moved on a circular trace over the specimen surface. This procedure allows to evaporate relatively large samples without generating deep craters. Formation of deep craters must be avoided because it is associated with the risk of liquid globule ejection disturbing molecular evaporation.

cw CO$_2$ laser beam

triple chopper

shutter

vacuum balance

Am

compensation circuit

vacuum chamber

fixed mirror

lens

ballistic specimen

window

viewing window for reading telescope

collector (guard window)
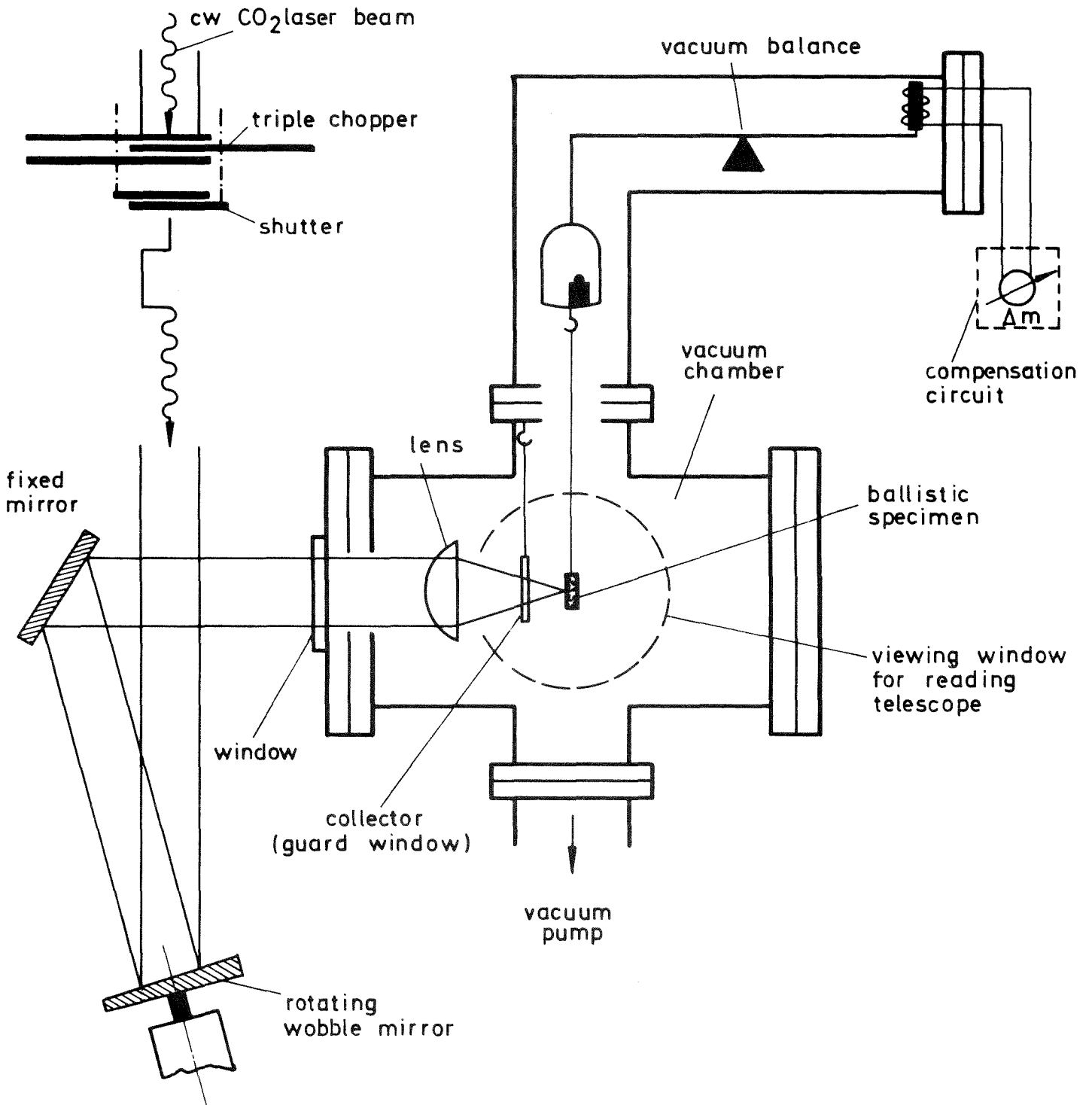
vacuum pump

rotating wobble mirror

Fig. 2   Measuring   principle

The lens is protected by a thin guard window of KCl, which is also suspended as a ballistic pendulum to measure the forward momentum of the impinging vapor jet. Both the recoil momentum of the target and the forward momentum of the vapor jet are determined by measurement of the pendula amplitudes, using a reading telescope and a photo camera, respectively. The forward momentum of the total vapor jet equals the recoil momentum of the target specimen. However, of the forward momentum only the portion is measured which is transferred to the collector window in the fixed space angle determined by the dimension and distance of the collector window. In this way, the ratio of the two momenta measured gives an indication of the flow structure of the vapor jet.

The recording system used is shown in Fig.3. By means of the camera the mode of evaporation can be checked in addition and the geometry of the vapor plume can be verified. In particular, photographic recording allows precise measurement of small amplitudes. This is important for the extension of experiments to evaporation temperatures below the boiling point, which imply smaller recoil momenta. The mass evaporated from the specimen is determined by weighing the specimen with the vacuum microbalance immediately before and after the impact of the laser pulse. To determine the evaporation area the specimen is inspected microscopically and ceramographically.

The fast photomultiplier pyrometer is presently used to determine the time of evaporation. Later on, the evaporation temperature will be determined by this pyrometer alternatively to the gasdynamic approach, especially in the temperature range below 4000 K. However, before the spectral emissivity of liquid UO_2 must be measured.

reading telescope
observing collector
amplitude

transparent
collector

rectangular
CO_2-laserpulse

specimen

lens

camera observing
vapor plume
and
pendulum amplitude

fast pyrometer
measuring focus
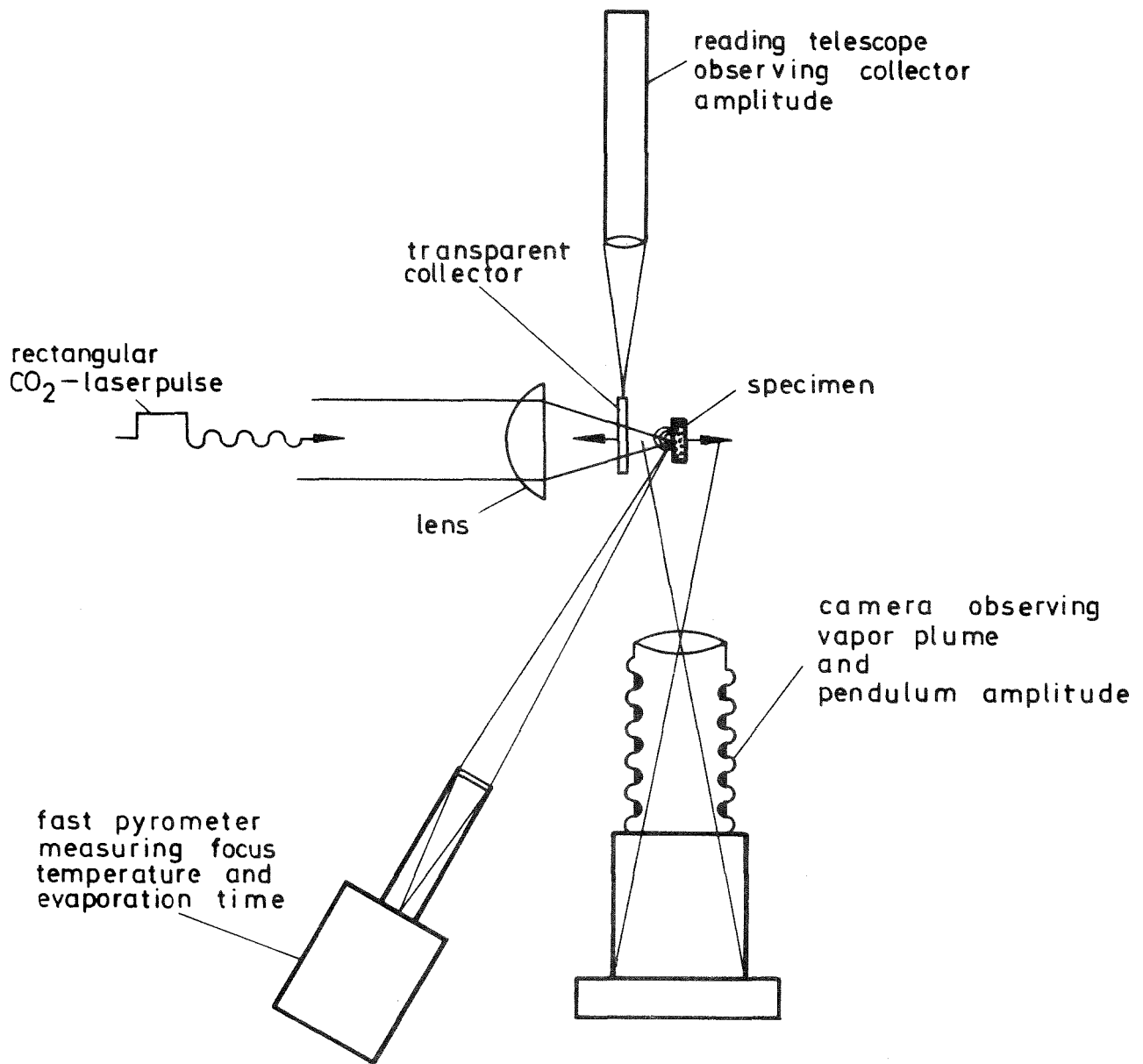temperature and
evaporation time

Fig. 3   Recording   system

From the mass loss of the target specimen obtained by weighing and from the measured evaporation time and area we get information on the mean mass flow rate. From the amplitude of the specimen pendulum and from the change in target mass we determine the velocity of the vapor jet and the reaction pressure of the jet on the target, averaged over the time of evaporation. With these quantities it is possible to derive in a first approach the vapor pressure of the specimen as a function of temperature.

As an illustration we indicate some typical values of the quantities measured in the evaporation experiments with UO_2 specimens. Depending on the laser impact on the specimen and on the mass of the specimen pendulum, pendulum amplitudes have been measured between 0.5 and 10 mm. The recoil momenta are between 0.5 and 5 gcm/s. Evaporation periods of 1 to 10 ms are chosen. The evaporation areas are between 10^{-4} and $5 \cdot 10^{-3}$ cm^2 in size and evaporated masses weigh between 10 and 100 μg.

Fig.4 is a photo of the apparatus showing, from left to right, the laser, the optical bench with the chopper-chutter system and the mirror system, and behind it the vacuum chamber with the microbalance.

Fig.5 once more shows the vacuum chamber with the microbalance fixed on top of it, the photo camera on the right behind the chamber, and the photomultiplier pyrometer in the foreground.

Fig.6 is a look into the interior of the chamber. We see the specimen pendulum, the KCl collector window, and the lens.
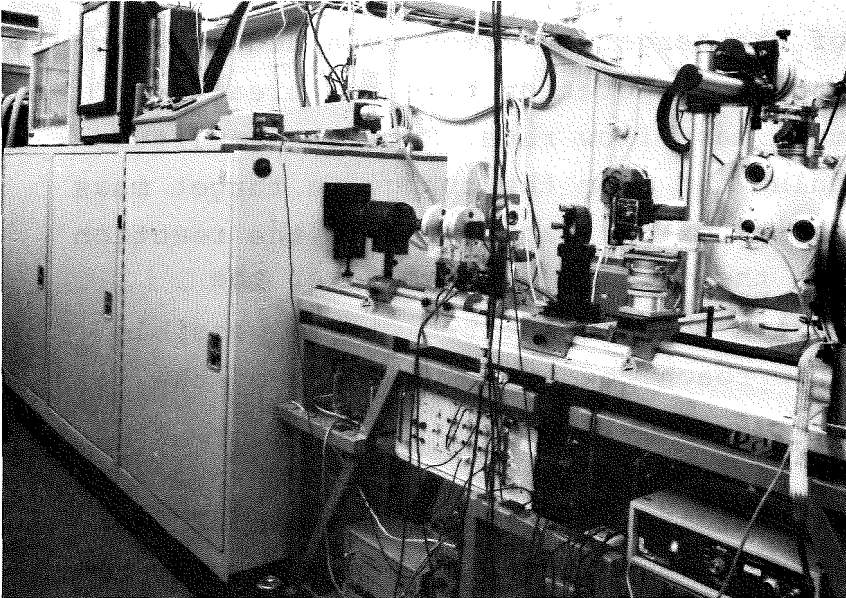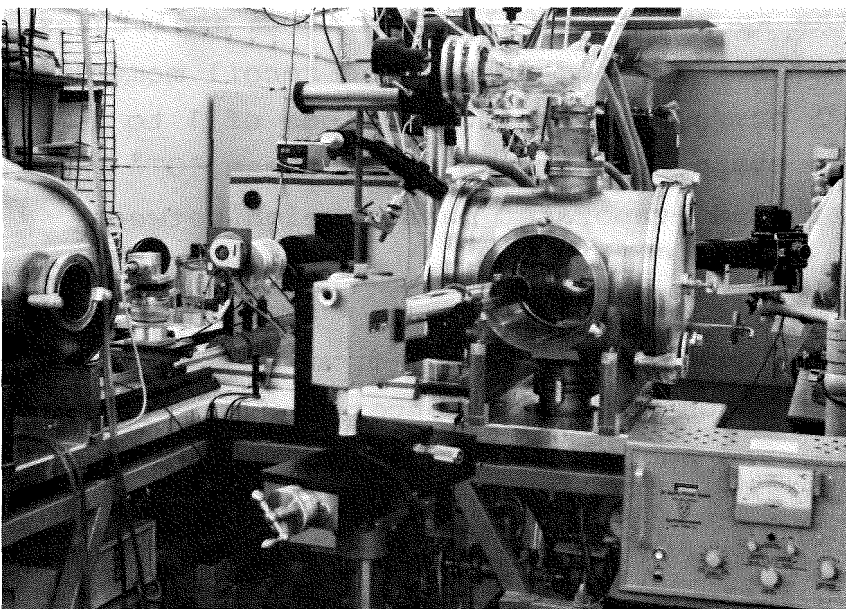
Fig. 4

Photo of the apparatus
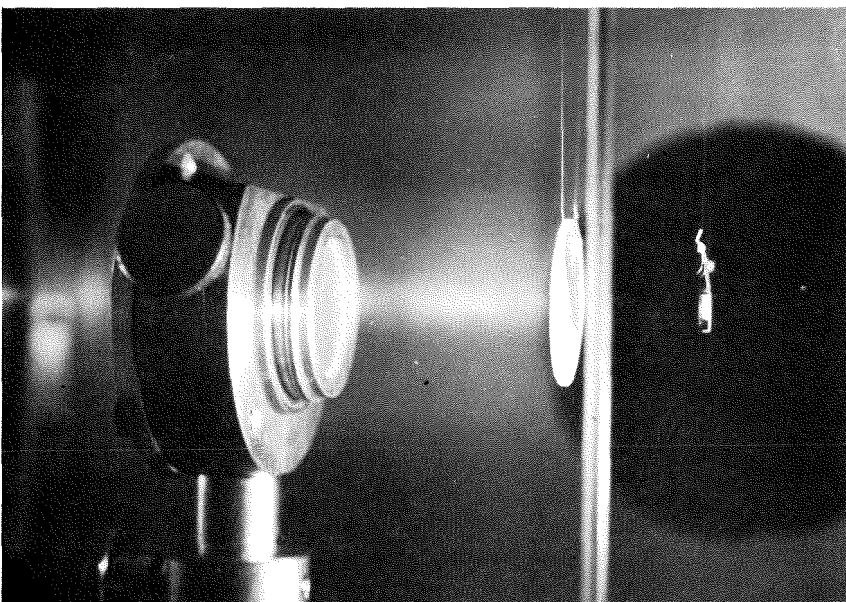

Fig. 5

Photo of the vacuum chamber

Fig. 6

Photo inside the chamber
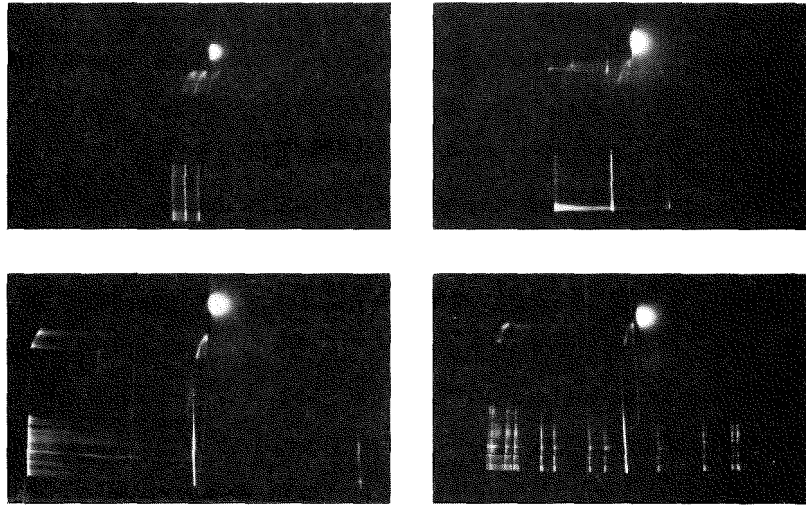
Fig. 7   Series of photos of UO$_2$ vapor
plumes and related pendulum
amplitudes for different laser
shots
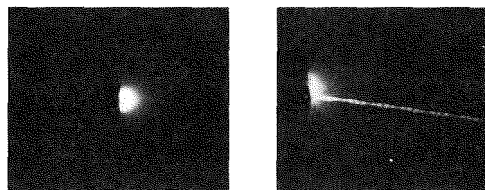

Fig. 8   UO$_2$ vapor plumes

In Fig.7 some photos of the specimen pendulum are given,
which show the vapor plumes and the pendulum amplitudes of
different laser shots. The amplitudes are made visible by
an illuminated platinum wire fixed at the foot of the specimen
holder. By this means the amplitudes can be measured. More-
over, a distinction can be made between well determinable and
wrong shots, e.g., an unsuccessfull experiment is shown in
the right-hand figure of the lower series where a tilting
oscillation of the specimen is superimposed to the pendulum
amplitude. Fig.8 shows two further photos of vapor plumes
produced in the experiments, the second is an example of
a shot which failed because particles of solid or liquid ma-
terial are ejected from the crater due to thermal stresses
in the specimen.

Fig.9 shows some photos of laser produced craters on UO_2
specimens. The laser focus was moved on the specimen surface
along circular traces of 1 to 2 mm diameter at velocities
between 0.1 and 1 mm/ms.

The lower crater photos are examples of defocused laser
shots with less power density obtained by imcomplete tur-
ning of the focus and a fixed focus, respectively.

The velocity of focus movement on the specimen surface is
restricted by the rate of heating of the target surface
toward the equilibrium evaporation temperature. This means
that the duration of local exposure to the laser beam must
be kept long compared to the heating-up period. This corre-
lation is illustrated on Fig.10 which gives the result of
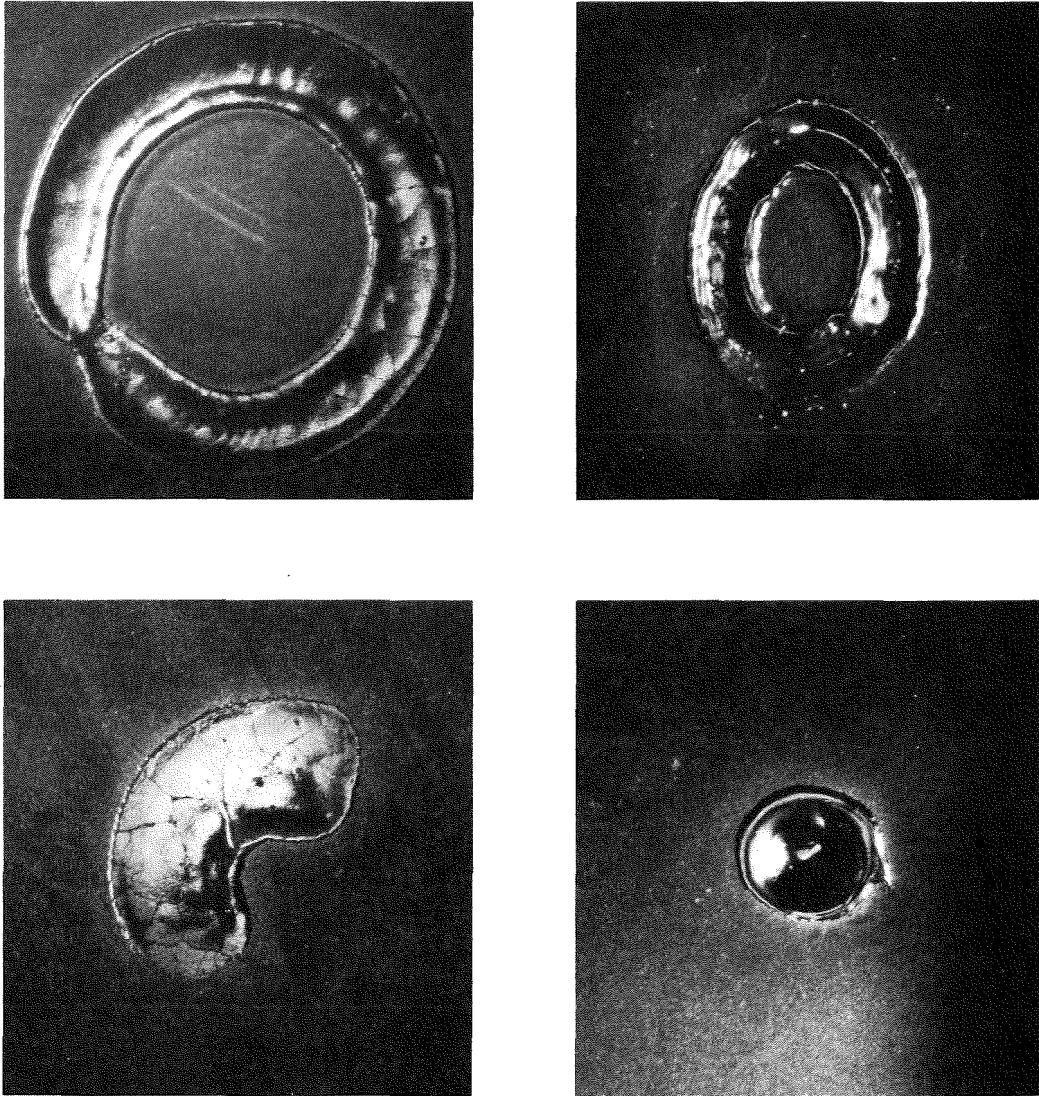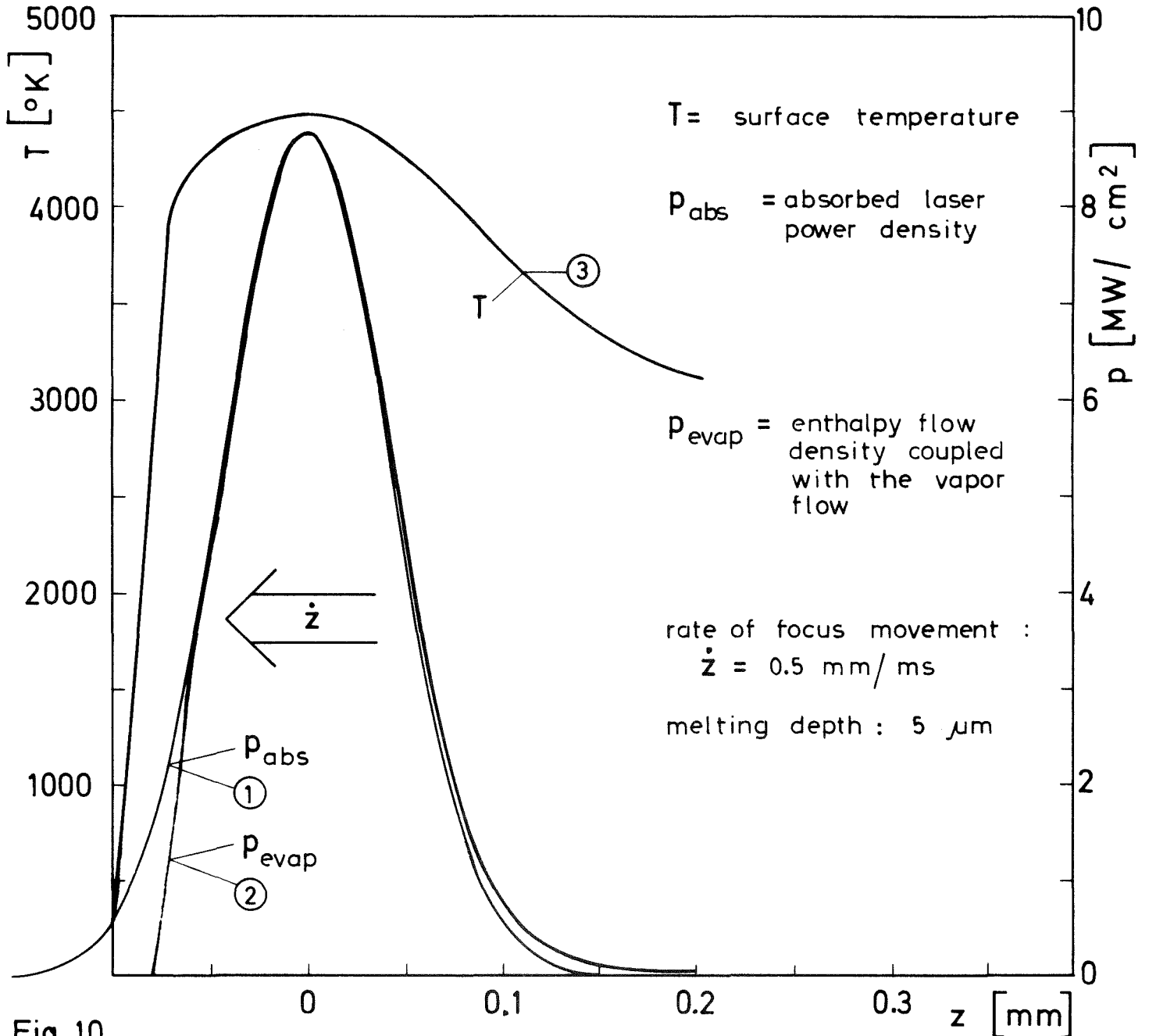a model calculation [18].

Fig. 9 Crater traces on UO_2 specimens

Fig. 10

Profiles of absorbed laser power density, surface temperature, and enthalpy flow density generated by a Gaussian laser focus moving on a UO_2 surface

In this example the laser focus is assumed to move on a
UO_2 surface from the right to the left side at a rate of
0.5 mm/ms. Curve 1 is the Gaussian profile of the absorbed
laser power density. In the temperature equilibrium the
enthalpy flow density P_{evap}, curve 2, carried away by the
vapor flow balances the absorbed laser power density. Curve 3
gives the development of the surface temperature along the
focus trace.

Fig.11 shows the temperature distribution in the laser
generated crater represented by means of isothermal lines.

It reveals to what extent the temperature distribution
could be distorted by the moving focus in the given example.
The isotherms in front of the moving focus appear squeezed
due to the time lag of heating. But, as can be seen, the
main part of the 1/e focus cross section shows a nearly
concentric temperature distribution.

Now we shall consider briefly the effects occuring in the vapor
jet formed at the surface undergoing evaporation during the
laser heating.

In the pressure-temperature range of interest, the laser-
generated vapor plume near the focus is so large and dense
that its state is dominated by collisional interaction of
the vapor molecules, for example, the mean free path in
UO_2 vapor at a pressure of 10 bar is about 0.1 µm. This im-
plies a gas-dynamic vapor flow.

It can be shown that the velocity of a vapor jet flowing
into a vacuum near the evaporating surface accelerates to
the local velocity of sound. With increasing distance from
the surface, the velocity increases to a supersonic level
and can reach a maximum value determined by the initial
enthalpy of the gas, while the pressure, temperature and
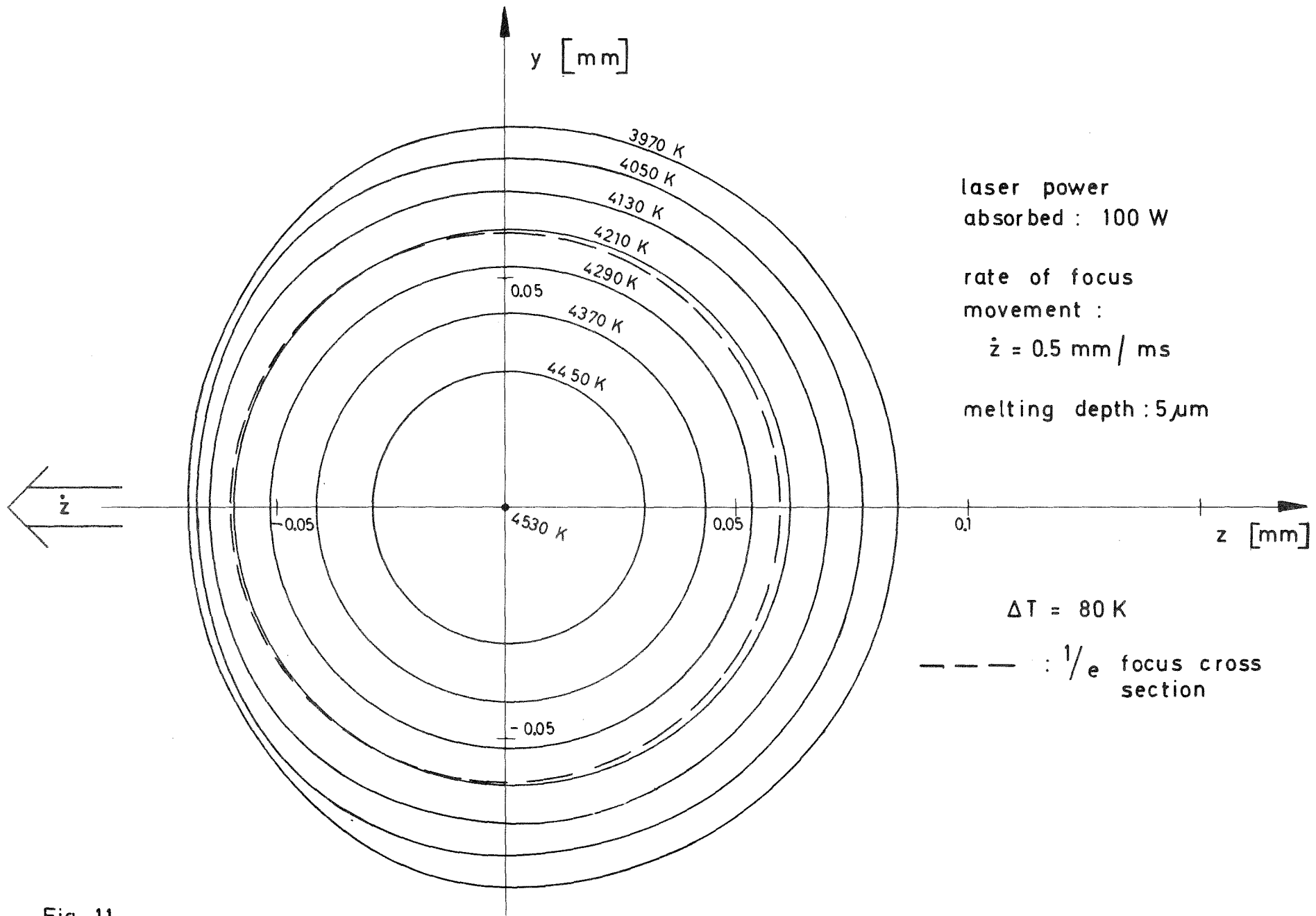density in the jet decrease.

Fig. 11

Temperature distribution in the laser crater generated by a moving Gaussian laser focus

This is confirmed by our experimental results: - In our laser evaporation experiments we have measured supersonic velocities of the vapor jet. This agrees with similar observations of several other authors as Anisimov et al. [23], Krokhin [24] and others. So, there must be an intensive gas-dynamic interaction in the vapor flow. Under the conditions of our experiments the vapor expands adiabatically and reaches its final velocity as a result of some 100 collisions per molecule.

Because the pulse duration is much longer than the time-of-flight of about 1 μs of the vapor during its gas-dynamic expansion, the vapor flow is quasi-stationary. This means that during the evaporation pulse the vapor jet acts upon the specimen like a stationary rocket thrust.

The task is now to determine the required vapor pressure and the evaporation temperature from the measured reaction pressure of the vapor jet and from the mass flow rate at the flow-off cross section. Fig.12 shows some simple relations between the measured quantities. The effective final velocity, w_{jet}^{final}, of the vapor is directly obtained from the measured mass rate $\dot{m}$ and thrust $\dot{I}$ with the simple rocket formula, given by Eq.(2), which holds for a one-dimensional jet.

$$(2) \qquad \dot{I} = \dot{m} \, w_{jet}^{final}$$

The supersonic final velocity w_{final} of the vapor jet yields direct information on the evaporation temperature required because this velocity is related to the enthalpy decrease of the vapor during its adiabatic expansion in the gas dynamic flow region.
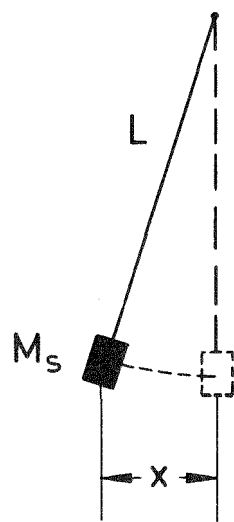
ballistic pendulum

L : pendulum Length

M_s : specimen mass

x : pendulum amplitude

g : acceleration of gravity

τ : evaporation - pulse time

$\dot{m}$: rate of evaporated mass

w_{jet}^{final} : final jet velocity

f : flow - off cross section at the focus

thrust : $\dot{I} = M_s \cdot \dfrac{x}{\tau} \sqrt{\dfrac{2g}{L}}$

(2) $\dot{I} = \dot{m} \cdot w_{jet}^{final}$

reaction pressure : $\dot{I}/f$

mass flow rate : $\dot{m}/f$

Fig. 12   Ballistic pendulum

Eqs.(3) to (6) describe the energy balance of the gasdynamic expansion of the vapor.

$$(3) \qquad \Delta H = H_{initial} - H_{final} = \frac{1}{2} M \cdot w^2_{final}$$

ΔH : enthalpy decrease

M : average molecular weight

$$(4) \qquad \Delta H = (f_{relax} + 2) \cdot R(T_{evap} - T_{final})/2, \quad T_{final} \approx 0$$

f_{relax} : number of degrees of freedom taking part in relaxation

T_{evap} : evaporation temperature

$$(5) \qquad \frac{M}{2} w^2_{final} = (f_{relax} + 2) \frac{R(T_{evap} - T_{final})}{2}$$

w_{final} : final velocity of the vapor

$$(6) \qquad w_{final} = K \cdot w^{final}_{jet}, \qquad K = K(f_{relax}) = K(\gamma)$$

The relation between the enthaply decrease ΔH and w_{final} is shown in Eq.(3) and (4). The enthalpy decrease depends on the actual number of degrees of freedom f_{relax} taking part in relaxation into the kinetic flow energy. A difficulty is that, in general, not all thermally excited degrees of freedom transfer their enthalpy during such gasdynamic expansion. However, when the amount of f_{relax} is known, the energy balance Eq.(5) clearly relates the evaporation temperature to the final velocity of the vapor.

Another difficulty is the fact that the real final velocity
of the vapor introduced in Eq.(5) is not identical with the
measured effective velocity of the jet determined by Eq.(2).
The actual velocity is somewhat larger than the measured
quantity. This is due to the spatial distribution of the
supersonic flow which is forward directed but still has a
radial component. The final velocity of the vapor is con-
nected to the measured effective jet velocity by the coef-
ficient K in Eq.(6). To find this coefficient we must have
sufficient knowledge of the flow structure and the con-
ditions of the jet formation. We shall try to obtain in-
formation about these conditions from a model based on
rarefied gas-dynamics.

III. Model of Evaluation

Fig.13 shows schematically the evaporation crater formed
by the focused laser beam. The vapor escapes from the liquid
surface of the molten material and expands over a very short
distance up to Mach1 velocity, to change subsequently into
a supersonic flow. The latter is now a free molecular flow
at a distance of some focus diameters. Speaking in terms of
gas dynamics we can describe the laser evaporation crater as
a "sonic orifice", i.e., a source of gas effusion with Mach1
velocity.
Ashkenas and Sherman investigated the flow structure of
a supersonic free jet during its unconfined expansion from
a sonic orifice [25]. They have found that the angular mass
distribution of the jet fits a $\cos^2$ distribution as given in
Eq.(7).

(7) $\qquad \rho(r,\theta) = \text{const} \cdot \cos^2 (\frac{\pi}{2\phi} \cdot \theta)$,
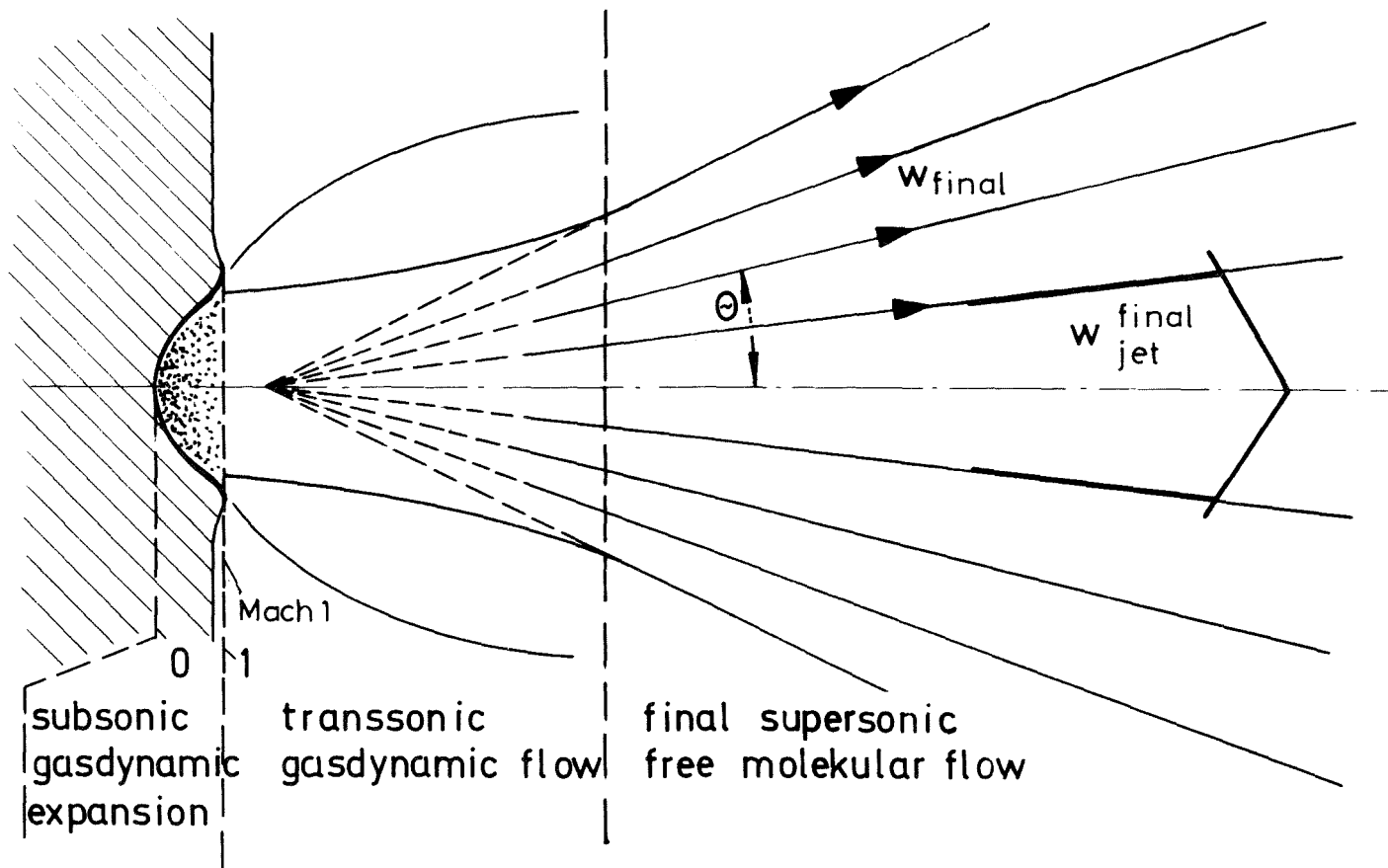
$$\phi = \phi(f_{relax})$$

Fig. 13   Schematical   figure   of   flow   geometry

This distribution, which is borne out by experiment, also depends on the actual number of degrees of freedom, f_{relax}, having participated in the relaxation into kinetic flow energy. The details of flow in the source region have been found to be of little influence on the flow structure in the super-sonic region, that is more than one source diameter down-stream. Therefore we can expect that in a first approach this theory is also applicable to our supersonic vapor flow.

Our measuring technique allows to check in a simple way the structure of the laser generated vapor jet by measure-ment of the forward momentum of the vapor which impinges within a defined space angle on the collector window ad-justed at a fixed distance from the specimen. Considering the ratio of the momentum transferred to the collector window to that of the recoil on the specimen, we found the ratio to correspond quite well to the $\cos^2$ distribution for the condition $f_{relax} = 5$; i.e., that 5 degrees of freedom take part in relaxation. The condition $f_{relax} = 5$ is reason-able for a gas dynamic UO_2 vapor flow as generated in our experiments. The collision number in the focus region is about 100. According to relaxation experiments by Hagena and Obert [26] this number of collisions is sufficient to transfer the translational and rotational heat of the mole-cular vapor into kinetic jet energy, but is insufficient to de-excite the vibrational levels.

Thus, the coefficient K in Eq.(6) can be obtained from inte-gration over the $\cos^2$ distribution function with the relax-ation condition $f_{relax} = 5$. This yields K=1.38. The magnitude of the real final velocity w_{final} of the vapor flow – which is equal in all stream lines – follows from the measured effective velocity w_{jet}^{final} by multiplication by this value of K. From this final velocity we get the knowledge of the evaporation temperature at the liquid surface.

The measured quantities involve the gas-dynamic expansion of the vapor. We have to look now for relationships correlating the measured quantities with the required thermodynamic quantities of the vapor before its expansion. From the theory of gas-dynamic Mach1 effusion we know the relationship between the gas density ρ_1 at the Mach1 flow cross section and the gas density ρ_0 before the beginning of the expansion [27]. This relationship is given in Eq.(8) where γ means the specific heat ratio equal to $(f_{relax} + 2)/f_{relax}$. Using in addition the well-known equation for the adiabatic expansion of a perfect gas Eq.(9) , we find the corresponding relationships for temperature and pressure.

$$(8) \qquad \rho_1 = \rho_0 \left(\frac{2}{\gamma+1}\right)^{1/(\gamma-1)} \text{ with } \gamma = c_p/c_v = \frac{f_{relax}+2}{f_{relax}}$$

$$(9) \qquad \frac{\rho_1}{\rho_0} = \left(\frac{p_1}{p_0}\right)^{1/\gamma} = \left(\frac{T_1}{T_0}\right)^{1/(\gamma-1)}$$

The local velocity of sound w_1 reached in the gas flow at the Mach1 cross section, Eq.(10), thus can also be related to the quantities valid before the expansion.

$$(10) \qquad w_1 = \sqrt{\gamma \frac{RT_1}{M}} = \sqrt{\frac{2\gamma}{\gamma+1} \frac{RT_0}{M}}$$

Combining Eq.(8) and (10) we finally obtain by Eq.(11) an expression of the mass flow rate at the Mach1 flow-off cross section. The cross section is located close to the evaporating surface.

$$(11) \qquad \frac{\dot{m}}{f} = \rho_1 w_1 = \rho_0 \left(\frac{2}{\gamma+1}\right)^{1/(\gamma-1)} \sqrt{\frac{2\gamma}{\gamma+1} \frac{RT_0}{M}}$$

So this equation already represents the first relationship correlating a measured quantity - i.e. the mass flow rate - with the required quantities of density and temperature of the vapor before its gas-dynamic expansion.

Measured quantities are : $\dot{m}/f$, $\dot{I}/f = p_{reaction}$, $\dot{I}/\dot{m} = w_{jet}^{final}$

Required quantities are: T_{evap} and p_s the saturated vapor pressure

The energy balance in the gas dynamic adiabatic expansion, Eq.(5), serves to determine the evaporation temperature. The required vapor pressure at the evaporating surface can be obtained either from the momentum transport or from the mass transport in the gas dynamic vapor flow. In the first case we have to correlate the measured reaction pressure to the static pressure at the liquid surface. To do this, we insert in the equation of the reaction pressure the corresponding gas dynamic expressions of the mass flow rate and jet velocity already derived, and get Eq.(12).

(12) $\quad p_{reaction} = \dfrac{\dot{m}}{f} \cdot w_{jet}^{final}$

$$= p_o \cdot \left(\dfrac{2}{\gamma+1}\right)^{1/(\gamma-1)} \cdot \dfrac{2\gamma}{\sqrt{\gamma^2-1}} \cdot \dfrac{1}{K(\gamma)}$$

If one would assume now that during evaporation the vapor layer immediately contacting the liquid surface would be fully saturated, then we could set the static pressure p_o equal to the saturated vapor pressure p_s. In this case the backscattering rate of the vapor would be in equilibrium with its flow rate off the surface. If, on the other hand, one would assume a free molecular evaporation without any backscattering and gas dynamic interaction of the vapor molecules, then we would have to double the reaction pressure for p_s. In fact, none of these two extreme conditions

is satisfied. We get

(13) $p_s = p_o$, if vapor layer at liquid surface is
         fully saturated,

$$= p_o \cdot \frac{2}{1+b} \Big/ \frac{\alpha}{1-b(1-\alpha)}, \text{ if not.}$$

We have neither a fully saturated vapor, because of the open
surface evaporation, nor a free molecular flow condition
because of the gas dynamic flow-off measured. The situation
can be described by introducing a numerical parameter b which
can be a number between 0 and 1 where b=1 belongs to the
saturated vapor condition with full backscattering. The real
state of the vapor at the phase boundary, i.e. before its
gas dynamic expansion, is not exactly known. So we take for
the vapor pressure evaluation a position in-between the two
extremes and introduce a backscattering parameter b=0.4   ·
taking into account the lack of balance of the vapor flow
rates to and from the surface. This causes a tolerable error
margin of about 30% in the resulting vapor pressure equal
to the plus and the minus side.

Now, one problem remains which is relevant to all open
evaporation experiments, the problem of the unknown vapor-
ization coefficient α which enters the expression $\begin{bmatrix} 13 \end{bmatrix}$
for p_s. In the first evaluation we have set $\alpha=1$. This seems
to be not so bad because one could expect α near 1 sup-
ported by the fact that the main portion of the vapor above
open evaporating UO_2 is made up of UO_2 molecules. Neverthe-
less, an appreciable uncertainty is left.

Introducing the parameters $f_{relax} = 5$, b = 0.4 and α = 1,
we obtain Eq.(14) which relates the required saturated vapor
pressure p_s to the measured reaction pressure.

(14) $\qquad p_s = 1.09 \cdot p_{reaction}$ with $f_{relax} = 5$, $b=0.4$, $\alpha=1$

Independent of the reaction pressure measured, there is another possibility to evaluate the vapor pressure, starting from the mass transport in the vapor flow, as given in Eq.(15).

(15) $\qquad \dfrac{\dot{m}}{f} = \rho_o \cdot \left(\dfrac{2}{\gamma+1}\right)^{1/(\gamma-1)} \cdot \sqrt{\dfrac{2\gamma}{\gamma+1}} \cdot \sqrt{\dfrac{R\ T_{evap}}{M}}$

$\qquad \rho_s = \rho_o \cdot \dfrac{2}{1+b} \Big/ \dfrac{\alpha}{1-b(1-\alpha)}$

With the ideal gas law and by inserting the same parameters as above in the expression for the vapor density ρ_s, we obtain Eq.(16) which now relates the required vapor pressure p_s to the measured mass flow rate and the evaporation temperature.

(16) $\qquad p_s = 2.09\ \dfrac{\dot{m}}{f} \sqrt{\dfrac{R\ T_{evap}}{M}}$ with $f_{relax} = 5$, $b=0.4$, $\alpha=1$

$\qquad p_s = \rho_s \cdot \dfrac{R\ T_{evap}}{M}$ (ideal gas law)

To evaluate the vapor pressure from the evaporation experiments we can use Eq.(14) and (16) either based on the measured reaction pressure or on the mass flow rate.

IV. Results

We consider now some results of laser evaporation experiments with UO_2. The resulting values for the saturated vapor pressure are given in Fig.14 as a function of the reciprocal temperature together with some curves extrapolated theoretically.

The cross marks represent the results of three series of laser evaporation measurements obtained at temperatures around 4200, 3950 and 3500 K. They belong to three different laser focus adjustments. The length of the cross lines indicates experimental scattering. The dotted cross mark denotes results given by Ohse et al. at temperatures of about 4600 K [15]. All these experimental results should be considered preliminary. This is true especially also for the lower result obtained from the experiments at temperatures below the boiling point.

These latter measurements are difficult because the evaporation rates and recoil momenta diminish thus becoming more sensitive to experimental errors. Also, the gas dynamic temperature evaluation could fail. But it is shown that the experiments are feasible and at least in connection with pyrometric temperature measurement they open up the possibility of joining the measurements which have been carried out up to 3400 K by Reedy and Chasanov with conventional transpiration technique [9]. An extrapolation of the latter measurements is shown by curve 2.

For comparison, theoretical curves are shown which exhibit the confidence interval covered by theoretical calculations of the total vapor pressure above UO_2. These curves are derived from different theoretical approaches extending from the principle of corresponding states, together with extrapolation of low temperature data, i.e. curve 1 [28] and curve 7 [29], and the significant structure theory of liquids, i.e. curve 4 [17], to computations derived from thermodynamic functions of the gaseous species and extrapolated UO_2 condensed phase data, i.e. curve 3 [30].
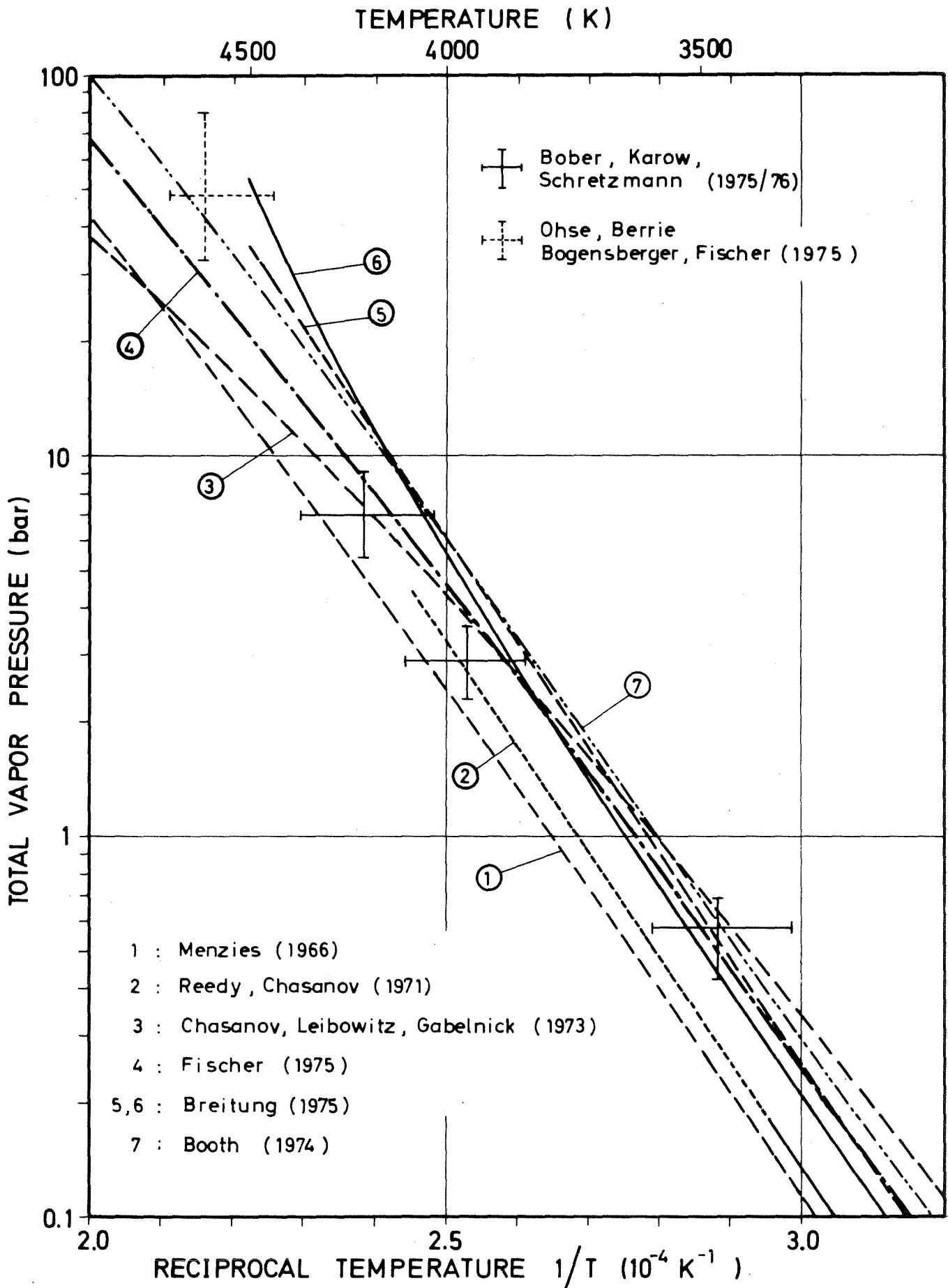
Fig. 14   p - 1/T diagram of UO$_2$, 3000 to 5000 K

The curves 5 and 6 [10] are derived from the law of mass ac-
tion with extrapolated data of both the free energies of for-
mation and of the oxygen potential. The different course of
these two curves is due to different conditions of evapora-
tion on which the calculations are based. Curve 5 has been
obtained for the case of total thermodynamic equilibrium
in a closed system underlying also the foregoing curves.
However, the solid line, curve 6, relates to the condition of
open surface evaporation where only local thermodynamic equi-
librium can be assumed in the phase boundary immediately at
the evaporating surface. Owing to preferential evaporation
of oxygen-rich components, the surface changes strongly in
its composition, which also alters the total vapor pressure
above the surface.

This is a matter of interest to us because this surface
depletion effect appears in all laser evaporation experiments
carried out on incongruently evaporating materials. It should
therefore be considered in the interpretation of results. The
actually measured vapor pressure can depart appreciably from
the equilibrium vapor pressure of the given specimen material.
This, in particular, applies to materials which are more com-
plex than uranium dioxide, like the (U,Pu) mixed oxides. In
the final part we shall deal with some questions belonging
to this topic. Before, we go on discussing briefly some pos-
sible error sources and evaluation limits of the measurements.

The risk that laser heating itself disturbs the measurements
by absorption of laser light in the vapor plume is not rele-
vant in the temperature range of our experiments. There is an
upper temperature limit given above 4500 K by the onset of
appreciable bound-free or free-free absorption or by total
reflection of the laser light in the partially ionized vapor.

The vapor pressure of oxide fuels can still be measured satis-
factorily up to about 4500 K. At higher temperatures the fuel
vapor would become an extremely dense plasma. This would
lead to afterheating of the expanding vapor by the laser beam,
i.e. the vapor temperature would become higher than the evap-
oration temperature.

Another strongly disturbing effect could be caused by inner
superheating of the molten fuel layer below the surface, which
could lead to ejection of molten material. There has been no
indication yet in our experiments of an onset of burst mode
evaporation. This has been proved in a separate experiment by
sampling the jet with an array of carbon-film coated grids.
No condensed or sprayed globules could be detected by inspec-
tion of the samples with an electron microscope of 20-$\overset{o}{A}$
resolution [12].

Besides, there is the uncertainty in the resulting vapor
pressures caused by the evaluation model used which does not
describe precisely enough the conditions at the evaporating
surface. This uncertainty becomes obvious by the not exactly
known values of the vaporization coefficient α and the back-
scattering parameter b.

However, because of the strong temperature dependence of the
vapor pressure, the temperature determination is the most
critical problem.It is difficult in the very high temperature
range, regardless of the method used. The determination of the
evaporation temperature from gas dynamic quantities used in-
volves a considerable uncertainty because it requires rather
good knowledge of the degree of relaxation in the gas and of
the jet structure.

Therefore, in the next series of experiments we measure the
evaporation temperature directly with a pyrometer in the
temperature range below 4000 K. In the lower temperature range
pyrometric measurement should be less affected by thermal
gradients below the evaporating surface, which contribute to

thermal radiation. So, it will be interesting to compare the
two evaporation temperatures resulting from pyrometric and
gas dynamic determinations and thus eventually to correct the
latter.

Before starting pyrometric measurements, we measure the spec-
tral emissivity of liquid uranium dioxide. An experiment with
an integrating sphere is going on in our laboratory.

As an illustration Fig.15 shows the measuring principle for
determination of the spectral emissivity both at the wavelengths
of a CO_2 laser and a He-Ne-laser. The latter has the same
wavelength as the pyrometer used in our experiments. The
specimen is fixed in the center of an integrating sphere.
With a CO_2 laser beam a surface spot of the specimen is
heated up to the liquid state and a modulated He-Ne-laser beam
is directed onto this liquid surface. The reflected portion
of the incident light at both wavelengths is measured by photo-
detectors after the light has been homogeneously distributed
in the sphere. For calibration of the sphere the specimen can
be replaced by a good optical mirror.

In the following part we deal with some questions belonging
to the surface composition changes during open surface evapo-
ration and to their consequences on the interpretation of
the vapor pressures of oxide fuels obtained from laser evapo-
ration experiments.

photo
detector

interference
filter for
HeNe-laser
line

HeNe-
laser beam

integrating
sphere

specimen

CO_2-
laser beam

variable angle
of incidence

focus adjustment

-34-

interference
filter for
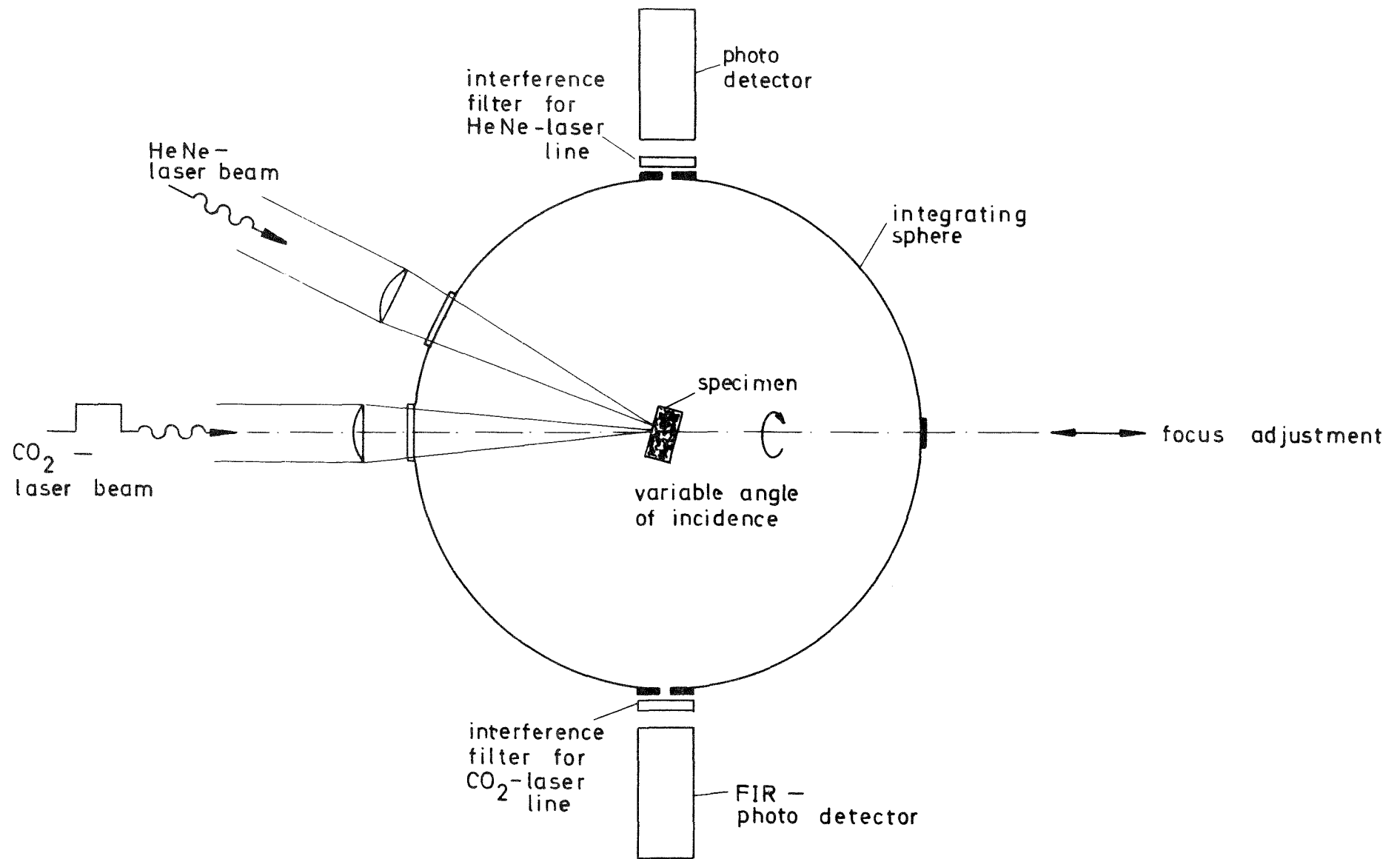CO_2-laser
line

FIR-
photo detector

Fig. 15   Intergrating sphere , measuring principle

# V. Interpretation of open-evaporation measurements

The following questions arise:
- To what extent and on which time scale do these changes in surface composition occur?
- What is their influence upon the vapor pressure of open-evaporating oxide fuel?
- How can vapor pressure measurements on liquid oxide fuels be interpreted:

To answer these questions calculations have been performed [10, 19, 31] which are based on thermodynamic data from the literature. This allows analysis of open surface-evaporation of uranium dioxide and uranium-plutonium mixed oxide fuel. Some of the results will be discussed here.

The evaporation behavior of stoichiometric uranium dioxide can be illustrated quantitatively by Fig.16. The upper figure shows a system of condensed UO_2 with the vapor phase consisting of 6 species. The O/U-ratio of the vapor phase is greater than that of the condensed phase. During open surface evaporation a net evaporation flux off the sample surface appears, which can be described by the velocity v at which the evaporating surface recedes.

With the onset of evaporation the higher O/U ratio of the gas phase is accompanied by an oxygen loss in the receding surface. This oxygen loss in the surface causes a diffusion flux of oxygen toward the surface so that an oxygen concentration profile develops in the condensed phase as a function of time. This concentration profile finally reaches a steady state which is determined by the recession velocity v of the phase boundary and the diffusion coefficient of oxygen D_{ox} in the condensed phase. The mathematical solution of the boundary value problem yields two characteristic quantities: A characteristic length D_{ox}/v which describes the final depth of oxygen depletion and a characteristic time D_{ox}/v^2
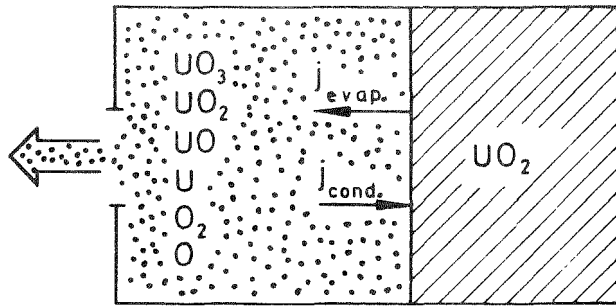
v : surface evap-
oration velocity

D_{OX}: diffusion coef-
ficient of oxygen
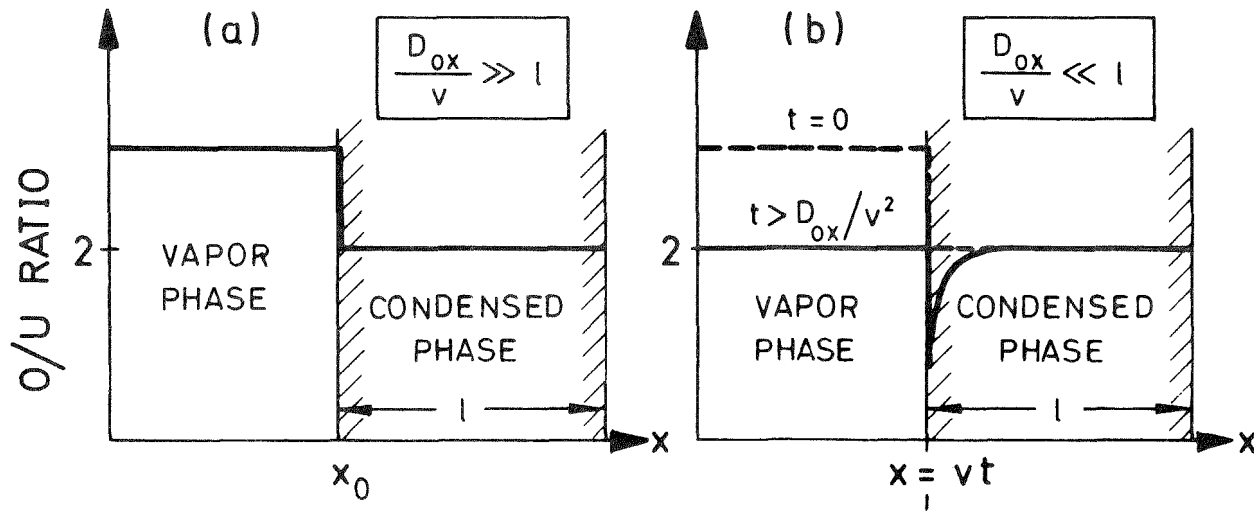
D_{OX}/v : characteristic length of oxygen depletion zone

D_{OX}/v^2 : characteristic time for reaching the steady state

Fig. 16   Evaporation modes of UO_2

indicating the period after which the concentration profile
can be regarded as independent of time.

In a practically closed static system as described by figure(a),
e.g. a Knudsen cell, the evaporation velocity is vanishingly
small. This means that the mobility of oxygen in the condensed
phase is sufficient to compensate incongruent evaporation so
that complete equilibrium is attained. The quotient D_{ox}/v
becomes greater than 1, the dimension of the specimen normal
to the evaporating surface. In this case the loss of oxygen
at the evaporating surface can be compensated from the whole
specimen.

In open evaporation of liquid UO_2, as shown by figure (b),
the net vapor flow, and hence the evaporation velocity, are
high. In this case only local thermodynamic equilibrium still
exists in the phase boundary immediately at the evaporating
surface. The surface becomes instantaneously depleted in
oxygen which cannot be restored by diffusion from the bulk.
Correspondingly, the oxygen content in the vapor phase de-
creases. At last, steady-state evaporation is reached for
which, based on the mass balance, the gross composition of
the vapor phase is congruent with the fuel composition of the
bulk, while the fuel surface is strongly hypostoichiometric.

This steady-state, forced congruent evaporation mode is
asymptotically reached after a transient evaporation period
of a few D_{ox}/v^2. Oxygen depletion in the steady-state reaches
a depth of a few D_{ox}/v, which is very small in comparison
with the thickness 1 of the condensed phase in all practical
cases of liquid UO_2 open evaporation.

Also in high-temperature evaporation of (U,Pu)-mixed oxide a
depletion of oxygen appears in the surface layer of the evapo-
rating material. But this oxygen depletion is coupled with
plutonium enrichment because the gas phase of mixed oxides con-
tain less plutonium than the condensed phase. This makes the
calculation more complex. It can be shown, however, that, as

in the case of UO_2, the highest diffusion mobility in the
condensed phase belongs to the oxygen, which again determines
the characteristic depth of the disturbed surface layer and
the time constant necessary to reach the steady-state,
forced-congruent evaporation mode.

It is obvious from these findings that during high-temperature
open-evaporation of oxide fuel the changes in surface compo-
sition lead to time-dependent partial and total vapor pressures.
Only in the steady state of forced congruent evaporation the
gross vapor composition is well defined but the actual surface
composition is unknown. This entails as a consequence that
the vapor pressure versus temperature measured in open sur-
face evaporation does not represent the equation-of-state of
the specimen in its given composition. It belongs to the
different composition of the evaporation surface, which
depends on the evaporation temperature.

To make clear this situation we shall consider some results
of the analytical solution of the boundary value problem.

From thermodynamic data the vapor composition can be calcula-
ted for every surface composition from the law of mass ac-
tion. This calculation assumes local thermodynamic equilibrium
at the phase boundary. The higher O/M ratio of the evaporation
flux causes the oxygen concentration in the receding surface
to decrease. Numerical coupling of the evaporation flux at the
phase boundary with the diffusion transport of oxygen in the
condensed phase yields both the actual surface composition
as a function of time and the transient development of the
oxygen concentration profile.

Fig.17 shows oxygen concentrations in a uranium dioxide and
in a hypostoichiometric uranium-plutonium mixed oxide specimen,
which are calculated under the condition of open surface evapo-
ration. As can be seen, the steady state distribution is
reached after some 500µs or 100µs at 3700 and 4000 K, respec-
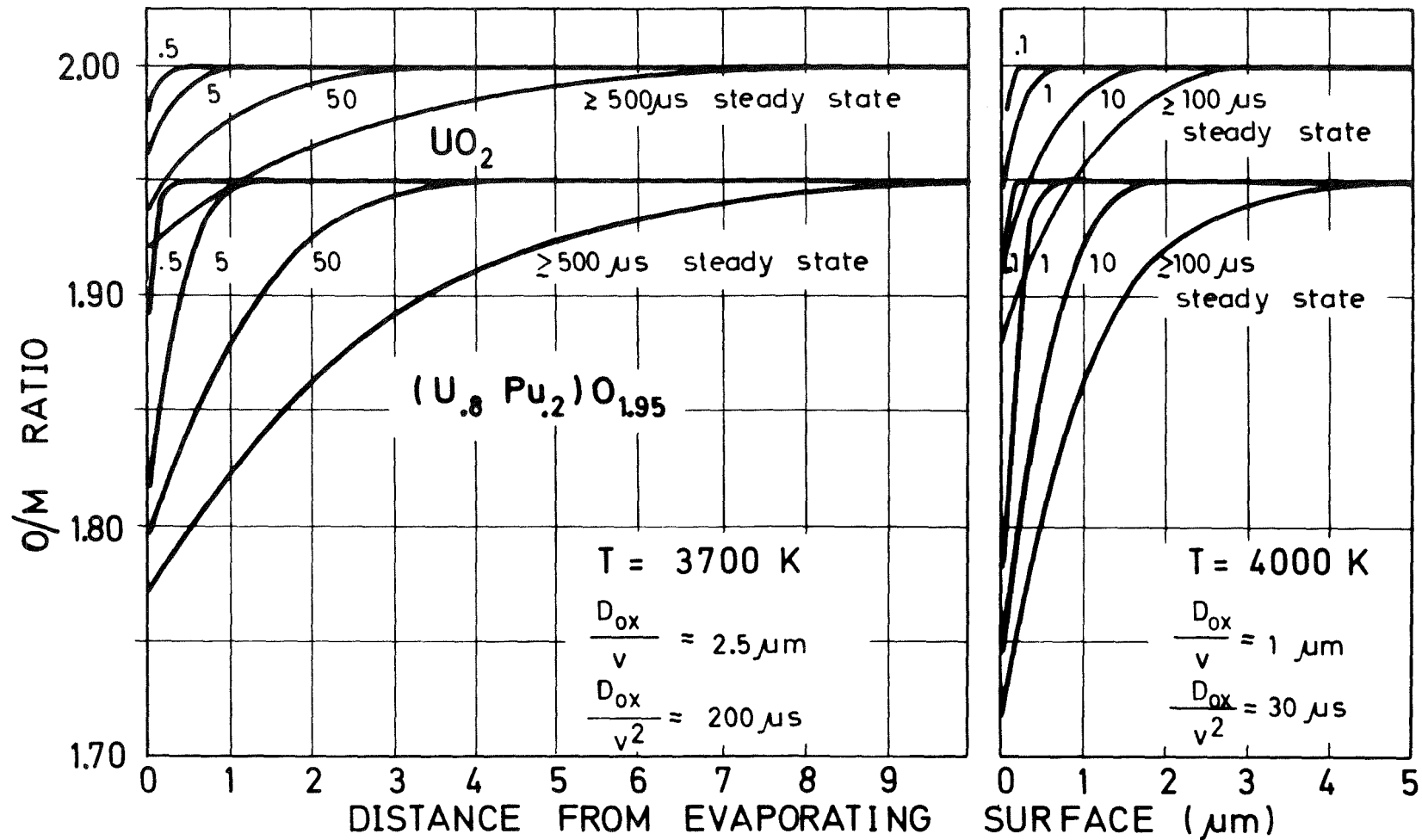tively. Immediately with the onset of evaporation the O/M

Fig. 17   Calculated   oxygen   concentrations   in UO_2 and $(U_{.8}Pu_{.2})O_{1.95}$
for   different   evaporation   times,
stationary   surface   compositions   at   4000 K : $UO_{1.88}$ and $(U_{.57}Pu_{.43})O_{1.72}$

ratio of the evaporating surface drops very quickly to low
values. The resulting oxygen depletion is enhanced in the
mixed oxide because of the higher oxygen potential. The cal-
culation gives surface compositions which become the more
hypostoichiometric the higher the evaporation temperature
is. At 4000 K, e.g. the O/M ratio falls to 1.88 in the
case of UO_2 and to 1.72 in the case of the mixed oxide con-
taining 20 mol% of plutonium oxide. The steady-state surface
compositions are in local thermodynamic equlibrium with the
forced-congruent vapor phase having an O/M ratio of the bulk
material, i.e. 2.00 and 1.95 respectively.

In the surface of the mixed oxide strong depletion in uranium,
i.e. enrichment in plutonium, occurs in addition. At 4000 K
the calculation gives a stationary surface composition of
$(U_{.57}Pu_{.43})O_{1.72}$ which is quite different from the bulk
composition.

The variation of the stoichiometric condition of the surface
obviously causes a variation of the total vapor pressure with
time. In Fig.18, the calculated pressure variation is shown
as a function of the evaporation time.

The resulting curves for 3700 K and 4000 K are normalized
to their initial values set to 100 %. These initial values
represent the total vapor pressures of the still undisturbed
evaporating surface, which are identical to the equation-
of-state pressure of UO_2 and the mixed oxide with O/M=1.95,
respectively. Owing to the drop in the oxygen content of the
evaporating surface, the transient vapor pressure falls very
rapidly to a minimum value and then approaches the final
vapor pressure of forced congruent evaporation.

The minimum pressure is caused by two competing effects:
With decreasing O/M ratio the oxygen partial pressure
and thus the total vapor pressure decreases; on the other
hand, the thermodynamic stability of the evaporating fuel
also decreases, which in the far hypostoichiometric range
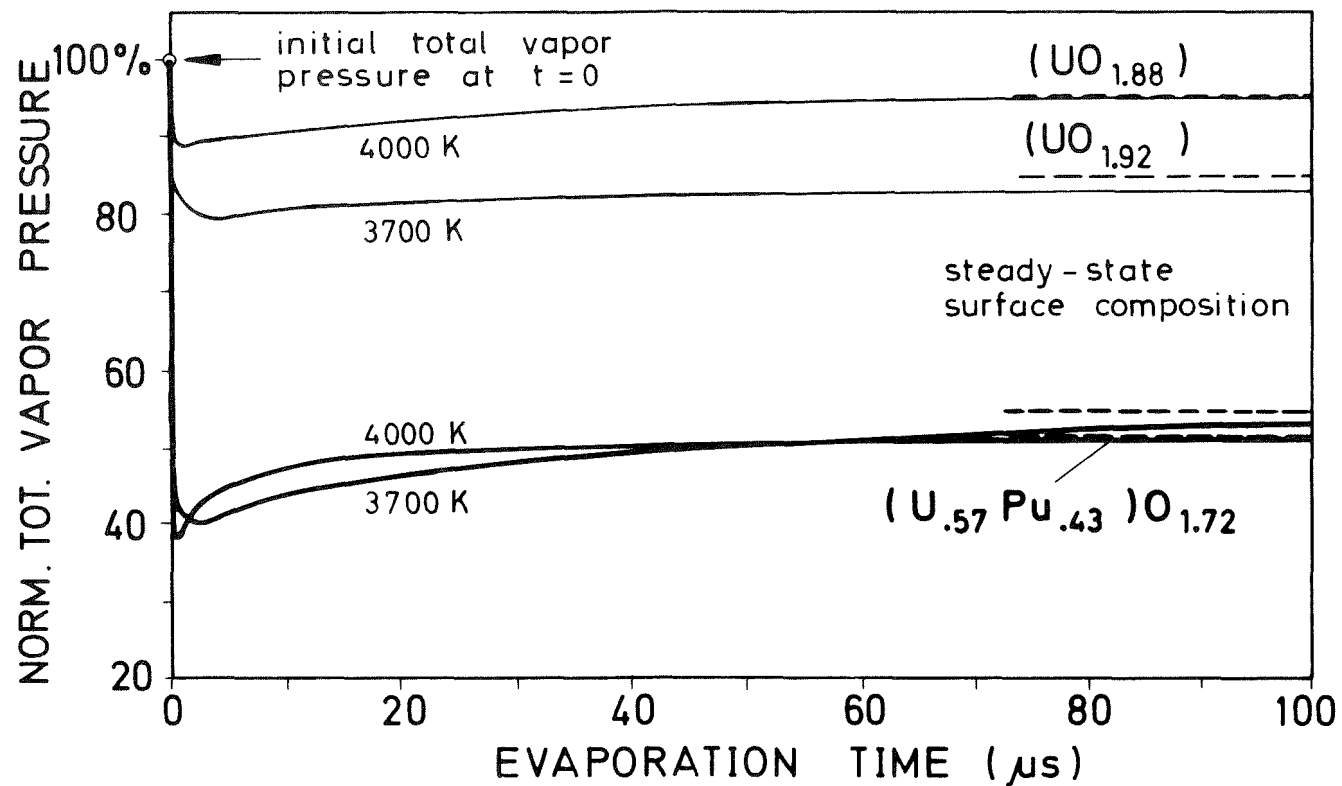again leads to a slight increase in the vapor pressure.

Fig. 18 Time dependent relative variation of the total vapor pressure of UO_2 and $(U_{.8}Pu_{.2})O_{1.95}$ under open evaporation condition

In case of the mixed oxide, the minimum transient vapor
pressure is less than half of the equation-of-state pressure
theoretically existing at the beginning. Measurement of the
stationary total vapor pressure under forced congruent evapo-
ration conditions calls in fact for an evaporation time which
is longer than the transient period. On the other hand, it
appears impossible to measure the equation-of-state pressure
of a liquid oxide fuel in its given composition also in short-
time evaporation experiments because of the rapid initial drop
of the vapor pressure.

Fig.19 shows vapor pressure curves log p versus the reciprocal
temperature of UO_2 and (U,Pu) mixed oxide. The solid lines
are calculated for the forced-congruent surface-evaporation
mode, the dashed lines are obtained for the total thermodynamic
equilibrium in a closed system representing the equation-of-
state pressure.

For comparison also the vapor pressure data evaluated from
laser evaporation experiments are indicated in the figures.
The cross marks represent our evaporation measurements with
uranium dioxide. The dotted lines are obtained by Ohse et al.
from a linear fit through their evaporation measurements and
through the equation-of-state pressure at the melting point.
The lines refer to uranium dioxide and (U,Pu) mixed oxide
with 20 mol% of plutonium oxide and an O/M ratio equal 1.95.

We turn to the calculated vapor pressure curves. The calcula-
tions yield in the case of uranium dioxide that the pressure
difference is relatively small between the two evaporation
modes up to temperatures of 4000 K, but becomes enhanced at
higher temperatures. The curve for forced congruent evapora-
tion has another slope than the equation of state. The reason
is that along the curve of forced-congruent evaporation not
only the temperature varies but also the composition of the
evaporating surface. Therefore, the slope of this curve does
not represent any real heat of evaporation. At some points
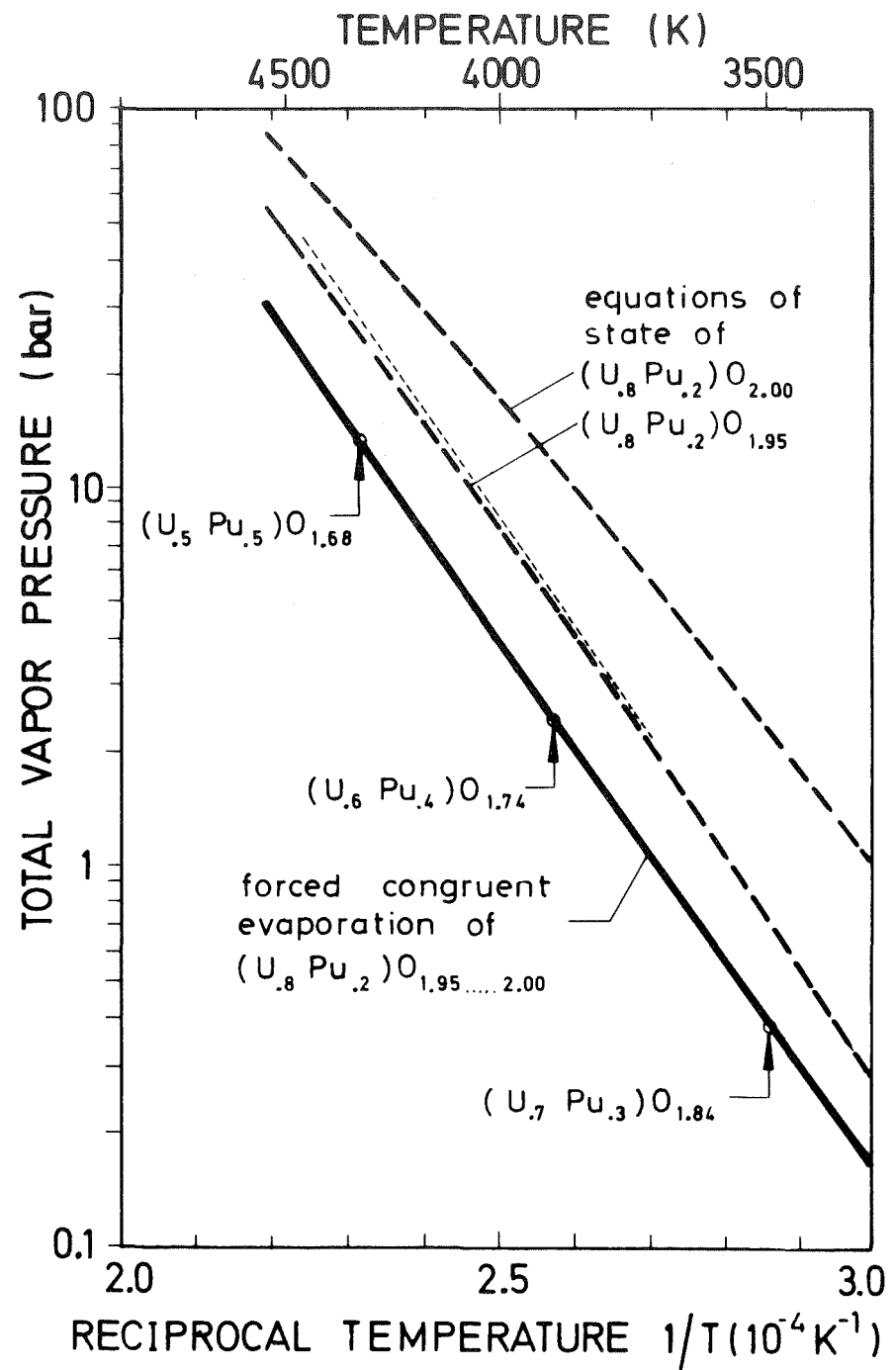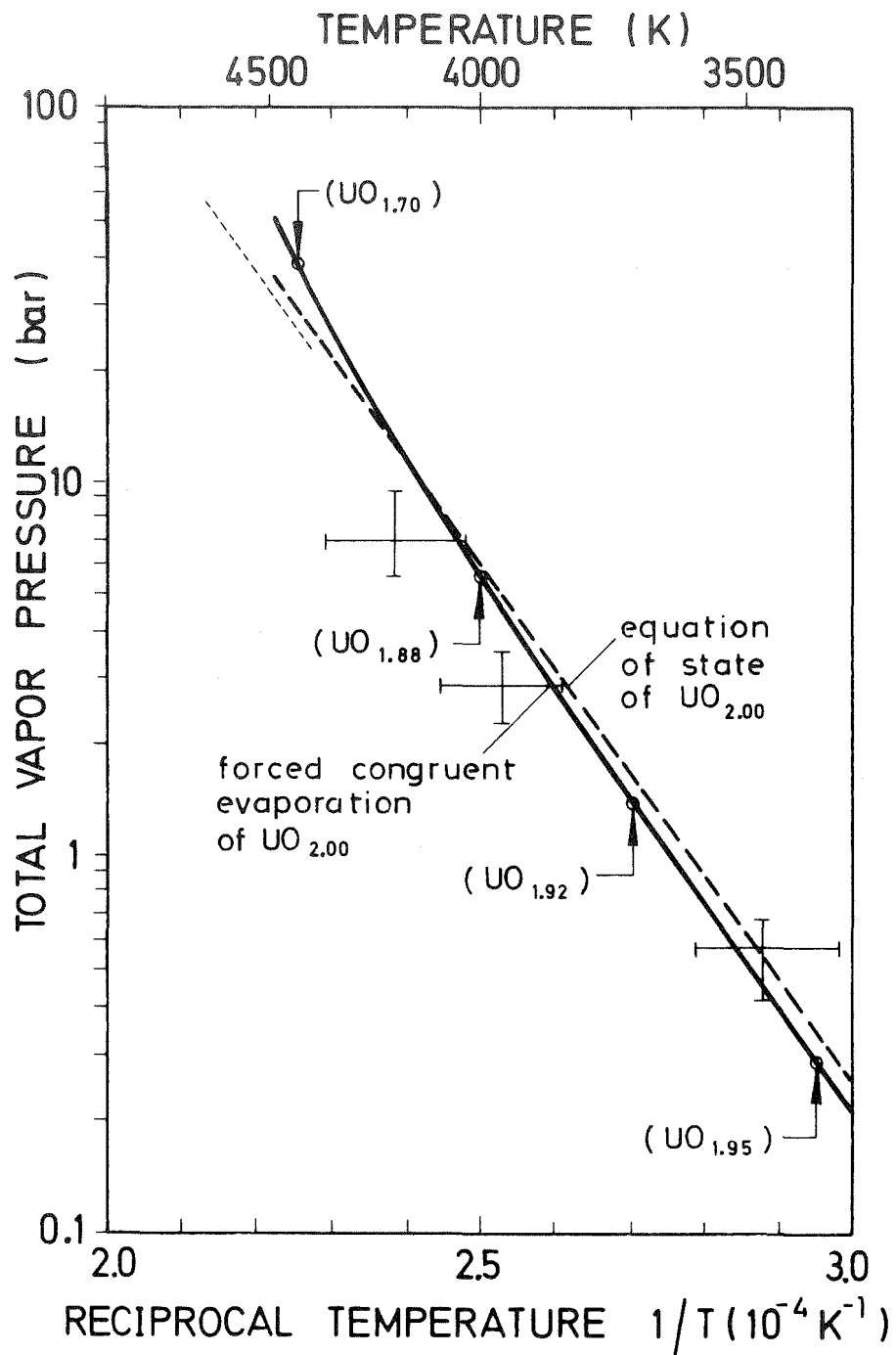the calculated compositions of the surface are indicated.

Fig. 19   p - 1/T diagram   of UO_2 and $(U_{.8} Pu_{.2})O_{2-x}$

- By contrast, the equation-of-state is univariant; this means that only the temperature is varying while the composition of the surface remains unchanged.

In case of the mixed oxide the vapor pressure curves have been calculated for the two stoichiometric conditions O/M=2 and O/M=1.95. These conditions have been chosen because the stoichiometry of the reactor fuel usually lies between these values. In fact, the results of the calculation yield two different lines for the equation-of-state. However, the vapor pressure curves for forced-congruent evaporation coincide on the bulk line shown. This means that this line is independent of the original O/M ratio. Contrary to the behavior of UO_2, the vapor pressures given by the equations-of-state differ substantially from the vapor pressure obtained for forced-congruent evaporation, i.e. by a factor between 2 and 7.

Because of the higher oxygen potential of mixed oxide, oxygen depletion in the evaporating fuel surface has a greater effect upon the oxygen partial pressure and the total vapor pressure than in the case of UO_2. The actual surface composition calculated for forced-congruent evaporation of the mixed oxide fuel is given by the values indicated along the vapor pressure curve. These values show the extent of the oxygen and uranium depletion in the evaporating fuel surface, both substantially increasing with the temperature. The depletion of uranium implies a strong enrichment of plutonium in the surface layer which can be considered to act like a filter impeding the evaporation of the uranium bearing species. This might plausibly explain why the total vapor pressure curve of the mixed oxide calculated for forced-congruent surface evaporation is even somewhat lower than that of uranium dioxide.

It should be noted that the theoretical results indicated remain basically unaffected by possible uncertainties in the thermodynamic input data used in the numerical analysis. Variations in the kinetic material data, such as the diffusion coefficient or the evaporation velocity, can only alter the

timescale of the transient vapor pressure range.

So we, reach the following conclusions.

The thermodynamic equation-of-state of any oxide fuel in its given composition cannot be measured practically in laser evaporation experiments, because at the very onset of intensive surface evaporation the evaporating surface is considerably changed in its composition.

Interpretable dynamic vapor pressure measurements on liquid oxide fuel can only be obtained in the steady-state of forced-congruent surface evaporation. Thus application of integrating measuring techniques requires evaporation times which are long in comparison with the transient evaporation period.

The measured vapor pressure curve can deviate appreciably from the theoretical equation-of-state of the bulk fuel. Besides this curve appears to be practically independent of the original O/M ratio.

For mixed oxides the surface vapor pressure could deviate by a factor of 2 to 7 from the equation of state. This fact must be considered in addition to the great systematic errors which still hinder the measuring methods.

The vapor pressure curve for open surface-evaporation of a liquid oxide fuel cannot, in principle, be expected to be linear in the form log p versus 1/T because every evaporation temperature produces another composition in the evaporating surface.

The required equation-of-state of liquid oxide fuel can be deduced from the measured vapor pressure curve of forced congruent evaporation only in a further step by thermodynamic calculations. This fact implies that still more measurements have to be made and requires great efforts in further laser evaporation experiments with oxide fuels.

Acknowledgment

We wish to thank R. Huber for the ceramographic preparations and for drawing the diagrams.

References

1. R.J.Ackermann, P.W.Gilles, R.J.Thorn,
    Chem.Phys.25 (1956) 1089

2. V.E.Ivanov, A.A.Kruglykh, V.S.Pavlov, G.P.Kovtun,
    V.M.Amonenko,
    Proc. IAEA Symp. on Thermodynamics of Nuclear Materials,
    Vienna (1962) 735

3. N.M.Voronov, A.S.Danilin, I.T.Kovalev,
    Vienna (1962) ibid. p.789

4. A.T.Chapman, R.E.Meadows, ORNL-Report 3587 (1964)

5. R.W.Ohse, J.Chem.Phys.44 (1966) 1375

6. A.Pattoret, I.Drowart, S.Smoes,
    Proc. IAEA Symp. on Thermodynamics of Nuclear Materials,
    Vienna (1967) 613

7. C.A.Alexander, J.S.Ogden, G.W.Cunningham,
    BMI-Report 1789 (1967).

8. M.Tetenbaum, P.D.Hunt,
    J.Nucl.Mater. 34 (1970) 86

9. G.T.Reedy, M.G.Chasanov,
    J.Nucl.Mater. 42 (1972) 341

10. W.Breitung, KFK-Report 2091 (1975)

11. R.J.Ackermann, M.S.Chandrasekharaiah
    Proc. IAEA Symp. on Thermodynamics of Nuclear Materials
    1974, Vol.2, Vienna (1975) p.3

12. M.Bober, H.U.Karow, K.Schretzmann,
    Proc. IAEA Symp. on Thermodynamics of Nuclear Materials 1974,
    Vol.1, Vienna (1975) p. 295

13. M.Bober, H.U.Karow, K.Schretzmann,
Nuclear Technology 26 (1975) 237.

14. M.Bober, W.Breitung, H.U.Karow, K.Schretzmann,
Atomwirtschaft 20 (1975) 175

15. R.W.Ohse, P.G.Berrie, H.G.Bogensberger, E.A.Fischer,
Proc. IAEA Symp. on Thermodynamics of Nuclear Materials
1974, Vol.1, Vienna (1975) p. 307

16. R.W.Ohse, P.G.Berrie, G.P.Brumme, P.R.Kinsman,
Proc. 5th Conf. on Plutonium and Other Actinides 1975,
Baden-Baden, Vol.1, North-Holland Publ.Comp. Amsterdam
(1976) p.191

17. H.G.Bogensberger, E.A.Fischer, P.G.Berrie, P.R.Kinsman,
R.W.Ohse, KFK-Report 2272 (1976)

18. M.Bober, H.U.Karow, K.Schretzmann, to be published

19. M.Bober, W.Breitung, H.U.Karow, K.Schretzmann,
J.Nucl.Mater. 60 (1976) 20

20. M.Bober, W.Breitung, H.U.Karow, K.Schretzmann,
Atomwirtschaft 21 (1976) 365

21. M.Bober, W.Breitung, H.U.Karow, K.Schretzmann,
KFK-Report 1275/2 (1975) 123-7

22. M.Bober, W.Breitung, H.U.Karow, K.Schretzmann
KFK-Report 1275/4 (1976) 123-12.

23. S.I.Anisimov, A.M.Bonch-Bruevich, M.A.El'Yashevich,
Ya.A.Imas, N.A.Pavlenko, G.S.Romanov,
Sov.Phys.Tech.Phys. 11(1967)945.

24. O.N.Krokhin,
In Laser Handbook (F.T.Arecchi, E.O.Schulz-Du Bois,Eds.)
Vol.2, North Holland, Amsterdam (1972) 1371.

25.   H.Ashkenas, F.S.Sherman,
      Rarefied Gas Dynamics (C.L.Brundis, Ed.) Vol.2, Academic
      Press, New York (1966) 84

26.   O.F.Hagena, W.Obert
      Institut für Kernverfahrenstechnik, Kernforschungszentrum
      Karlsruhe, private communication

27.   L.Bergmann, C.Schaefer,
      Lehrbuch der Experimentalphysik (neu bearbeitet v.
      H.Gobrecht), Bd.1, p.739, Berlin 1970

28.   C.Menzies
      UKAEA-Report TRG 1159 (D) (1966)

29.   D.L.Booth
      UKAEA-Report TRG 1759 (R/X) (1969) (Reprint 1974)

30.   M.G.Chasanov, L.Leibowitz, S.D.Gabelnick
      J.Nucl.Mater.49 (1973) 129

31.   W.Breitung
      KFK-Report 2240 (1976).